View metadata, citation and similar papers at core.ac.uk

brought to you by CORE

provided by Elsevier - Publisher Connector

International Journal of Solids and Structures 47 (2010) 2017–2033

Contents lists available at ScienceDirect

International Journal of Solids and Structures

journal homepage: www.elsevier.com/locate/ijsolstr

Nonlinear finite element analysis of inflatable beams made from orthotropic woven fabric

K.L. Apedo *, S. Ronel, E. Jacquelin, A. Bennani, M. Massenzio

Université de Lyon, F-69622 Lyon, France
INRETS, UMR_T9406, LBMC, F-69675 Bron, France
Université Lyon 1, Villeurbanne, France

ARTICLE INFO

Article history:
Received 3 November 2009
Received in revised form 26 February 2010
Available online 3 April 2010

Keywords:
3D inflatable beams
2D orthotropic woven fabric
Nonlinear finite element

ABSTRACT

This paper was devoted to the three-dimensional nonlinear finite element analysis of inflatable beams. The beams under consideration are made of modern textile materials and can be used as a load-bearing beams or arches when inflated. A 3D Timoshenko beam with a homogeneous orthotropic woven fabric (OWF) was proposed. The model took into account the geometric nonlinearities and the follower force resulting from the inflation pressure. The use was made of the usual total Lagrangian form of the virtual work principle to perform the nonlinear equilibrium equations which were discretized by the finite element method. Two kinds of solutions were then investigated: finite elements solutions for linearized problems which were obtained by the means of the linearization around the prestressed reference configuration of the nonlinear equations and nonlinear finite element solutions which were performed by the use of an optimization algorithm based on the Quasi-Newton method. As an example, the bending problem of a cantilever inflated beam under concentrated load was considered and the deflection results improve the existing theoretical models. As these beams are made from fabric, the beam models were validated through their comparison with a 3D thin-shell finite element model. The influence of the material effective properties and the inflation pressure on the beam response was also investigated through a parametric study. The finite elements solutions for linearized problems were found to be close to the theoretical results existing in the literature. On the other hand, the results for the nonlinear finite element model were shown to be close to the results for the linearized finite elements model in the case of high mechanical properties and the nonlinear finite element model was used to improve the linearized model when the mechanical properties of the fabric are low.

© 2010 Elsevier Ltd. All rights reserved.

1. Introduction

In the recent decades, structural applications with inflatable beams or arches with modern textile materials have been growing, requiring great effort on the development of analysis. The advantage of using modern textile materials for these beams and arches over conventional materials is that the former can be tailored to specific requirements of certain applications, easy to deploy, lightweight and have a low storage volume.

Nowadays, inflatable beams pose significant challenges to the analysts. In the numerical modelling of inflatable beams, significant prior research have been conducted.

Steeves (1975, 1978) has investigated the load–deflection behaviour of pressurized beams based on linearly elastic theory, and has developed a linear pressurized fabric beam element that included a pressure stiffening term. Quigley et al. (2003) and Cavallaro et al. (2003) have used this finite element to predict the linear load–deformation response of inflated fabric beams. However, the pressure stiffening term in Steeves's element treated the axial pressure resultant as an externally applied, stiffening tension force. This formulation predicted an unbounded increase in beam stiffness with increasing inflation pressure. Wielgosz and Thomas (2002, 2003) and Thomas and Wielgosz (2004) have studied the load–deflection behaviour of highly inflated fabric tubes and panels, and have developed a specialized beam finite element using Timoshenko beam theory. In their approach, the force generated by the internal pressure has been treated as a follower force which has accounted for pressure stiffening effects. Bouzidi et al. (2003) have presented theoretical and numerical developments of finite elements for axisymmetric and cylindrical bending problems of pressurized isotropic membranes. The external loading has been mainly a normal pressure to the membrane and the developments have been made under the assumptions of follower forces, large displacements and finite strains. The total potential energy has been minimized, and the numerical solution has been obtained by using an optimization algorithm. Suhey et al. (2005) have presented a numerical simulation and design of an inflatable

* Corresponding author. Tel.:+ 33 4 72 65 54 64; fax: +33 4 72 65 53 54.
E-mail address: komla.apedo@bvra.etu.univ-lyon1.fr (K.L. Apedo).

0020-7683/$ - see front matter © 2010 Elsevier Ltd. All rights reserved.
doi:10.1016/j.ijsolstr.2010.03.030

Nomenclature

• *Coordinates systems*

$(\underline{l}, \underline{t}, \underline{n})$	warp, weft, normal directions of the fabric
(X, Y, Z)	cartesian coordinates
ξ	reference coordinate
$(\underline{e}_X, \underline{e}_Y, \underline{e}_Z)$	unit vectors of the cartesian coordinates
$\varphi = (\underline{e}_Z, \underline{n})$	angle

• *Mechanical properties*

E_l	modulus of elasticity in $\underline{l}$ direction of the orthotropic fabric
E_t	modulus of elasticity in $\underline{t}$ direction of the orthotropic fabric
G_{lt}	in-plane shear modulus of the orthotropic fabric
v_{lt}	Poisson's ratio due to the loading in the $\underline{l}$ direction and contraction in the $\underline{t}$ direction
v_{tl}	Poisson's ratio due to the loading in the $\underline{t}$ direction and contraction in the $\underline{l}$ direction

• *Internal forces*

N	axial force
T_y, T_z	shear force along y and z axes
M_y, M_z	moments around y and z axes

• *Beam geometry*

l_ϕ	natural length of the inflatable beam
R_ϕ	natural radius of the inflatable beam
t_ϕ	natural thickness of the inflatable beam
l_o	reference length of the inflatable beam
R_o	reference radius of the inflatable beam
t_o	reference thickness of the inflatable beam
A_o	reference cross-section area of the inflatable beam
I_o	reference moment of inertia of the inflatable beam

• *Loads*

F	intensity of the service load
f	normalized load
F_X, F_Y, F_Z	components of concentrated loads
f_x, f_y, f_z	components of the distributed load
M_Y, M_Z	components of bending moments
F_w	wrinkling load

• *Pressure, pressure forces*

p	inflation pressure
p_n	normalized pressure
$F_p = p\pi R_o^2$	pressure force
N^o	axial force due to the inflation pressure

• *Kinematics*

$\underline{U}$	displacements field
u	axial displacement
v, w	deflections along Y and Z axes
θ_Y, θ_Z	rotations around Y and Z axes

• *Tensors*

$\underline{\underline{E}}$	Green–Lagrange tensor
$\underline{\underline{S}}$	second Piola–Kirchhoff tensor
$\underline{\underline{R}}$	rotation matrix

• *Functions*

δW^d_{ext}	external virtual work of the service load
δW^p_{ext}	external virtual work of the pressure load

open-ocean-aquaculture cage using nonlinear finite element analysis of isotropic membrane structures. Numerical instability caused by the tension-only membrane has been removed by adding an artificial shell with small stiffness. The finite element model has been compared with a modified beam theory for the inflatable structure. A good agreement has been observed between the numerical and theoretical results. Le Van and Wielgosz (2005) have introduced finite rotations and an energy approach which has built on the earlier work of Fichter (1966) to analytically study the bending and buckling of highly inflated isotropic fabric beams. Le Van and Wielgosz (2007) have discretized the nonlinear equations obtained in Le Van and Wielgosz (2005) to carry out a finite element formulation for linearized problems of highly inflated isotropic fabric beams. Their numerical results obtained with the beam element have been shown to be close to their 3D isotropic fabric membrane finite element and analytical results obtained in Le Van and Wielgosz (2005). Davids (2007) and Davids and Zhang (2008) have derived a Timoshenko beam finite element for nonlinear load–deflection analysis of pressurized isotropic fabric beams and the numerical examination of the effect of pressure on the beam load–deflection behaviour. The basis of their element formulation has been an incremental virtual work expression that has included explicitly the work done by the pressure. Parametric studies have been also investigated to demonstrate the importance of including the work done by the pressure in their models. More recently, Malm et al. (2009) have used 3D isotropic fabric membrane finite element model to predict the beam load–deformation response. Comparison between the finite element model-predicted load–deflection response and beam theory has been shown the accuracy of the conventional beam theory to load–deformation for the isotropic fabric airbeam. In these former works, the fabric used to manufacture the beams was always supposed to be isotropic whereas this character is not the best one for this material.

Few papers deal with the case of the inflatable beams made of orthotropic fabric. Plaut et al. (2000) have studied the effect of the snow and wind loads on an inflated arch in the assumption of linear thin-shell theory of Sanders. They have used this theory to formulate the governing equations, which include the effect of the initial membrane stresses. The material was assumed to have a linearly elastic, nonhomogeneous and orthotropic behaviour. Approximate solutions have been obtained using the Rayleigh–Ritz method. Any study of the influence of the fabric orthotropic character has not been conducted. More recently, Apedo et al. (2009) have used the earlier work of Le Van and Wielgosz (2005) to analytically study the bending and the wrinkling problems of inflatable beams made of 2D OWFs. They have shown the importance of taken into account the orthotropic character of the fabric even if the effective properties in the two principal directions (warp and weft) are close.

Consequently, there is a need to develop efficient numerical techniques for predicting the nonlinear load–displacement response of inflatable beams and arches made of a 2D OWF. In this paper, this need is addressed through the development of a 3D Timoshenko beam element for the nonlinear analysis of inflatable 2D OWF beams. The present paper extends the work done in Apedo et al. (2009). The nonlinear equilibrium equations obtained by the virtual work principle are discretized by the finite element method. Two kinds of solutions are then investigated: finite elements solutions for linearized problems and nonlinear finite element solutions. As an example, the bending problem of a cantilever inflated beam under concentrated load is considered. To show the influence of the material properties on the beam response,

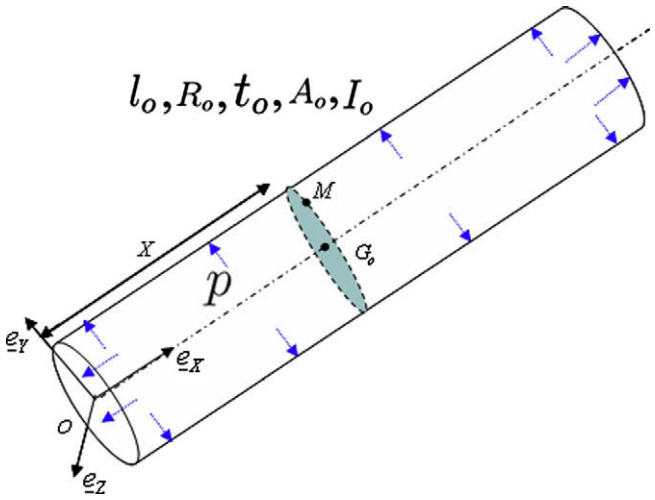

Fig. 1. 3D inflated beam.

one material with low properties and one material with high properties are used. A reference solution is performed using thin-shell finite element model. The paper closes with a summary and conclusions.

2. Basic equations

The theory used in this paper is already described in Apedo et al. (2009), but the formulation will be presented here for the sake of completeness. An inflatable cylindrical beam made of an OWF is considered (Fig. 1).

l_o, t_o, R_o, A_o and I_o represents respectively the length, the thickness, the external radius, the cross-section and the moment of inertia around the principal axes of inertia Y and Z of the beam in the reference configuration which is the inflated configuration.

p is the internal pressure. M is a point on the current cross-section and G_o the centroid of the current cross-section lies on the X-*axis*. The beam is then loaded. The following assumptions are made:

- the cross-section of the inflated beam under consideration is circular and maintains its shape after deformation, so that there are no distortion and local buckling. Indeed, many authors have studied the cross-section ovalization as a feature associated to the local buckling (Harursampath and Hodges, 1999; Houliara and Karamanos, 2006, 2010). In this paper, the model considers that no wrinkling occurs so that the ovalization problem is not addressed as done in many previous papers (Fichter, 1966; Le Van and Wielgosz, 2005);
- the rotations around the principal axes of inertia of the beam are small and the rotation around the beam axis is negligible as proven by Fichter (1966).

2.1. Kinematics

The kinematics laws for a beam allow to write (Batoz and Dhatt, 1990):

$$\underline{U}(M) = \begin{cases} u(X) + Z\theta_Y(X) - Y\theta_Z(X) \\ v(X) \\ w(X) \end{cases} \tag{1}$$

where $u(X)$, $v(X)$ and $w(X)$ are respectively the displacements of the centroid G_o of the current cross-section at abscissa X, related to the base (X,Y,Z) and $\theta_Y(X)$ and $\theta_Z(X)$ are the rotations of the current section at abscissa X around both principal axes of inertia of the beam respectively. The strains are nonlinearly related to the displacements through the Green–Lagrange strain $\underline{\underline{E}}$.

2.2. Constitutive laws

A homogeneous orthotropic hyperelastic material is considered.

The present model considers the Helmholtz free-energy function. Using previous works (Spencer, 1972, 1984; Aravas, 1992), the energy function $\Phi(\underline{\underline{E}})$ is expressed through a quadratic function of the components of $\underline{\underline{E}}$. Then, the components of the second Piola–Kirchhoff tensor $\underline{\underline{S}}$ are given by the nonlinear Hookean stress–strain relationships:

$$\underline{\underline{S}} = \frac{\partial \Phi}{\partial \underline{\underline{E}}} = \underline{\underline{\underline{C}}} : \underline{\underline{E}} \tag{2}$$

With $\underline{\underline{\underline{C}}}$, the elasticity tensor which depends on the material constants only.

To express the second Piola–Kirchhoff tensor related to the beam axes, we must firstly determine the components of the elasticity tensor related to the beam axes.

In this paper, we assume that the warp direction of the fabric coincides with the beam axis (see Fig. 2).

To describe the behaviour of an inflatable beam made from an orthotropic material, two coordinate systems are defined:

- A cartesian coordinate system related to the beam.
- A local warp-weft coordinate system related to each point of the membrane according to the principal directions of the fabric in which the orthotropic elasticity tensor is defined.

One can write (see Fig. 2)

$$\begin{cases} \underline{l} = \underline{e}_X \\ \underline{t} = \underline{e}_Y \cos\varphi + \underline{e}_Z \sin\varphi \\ \underline{n} = -\underline{e}_Y \sin\varphi + \underline{e}_Z \cos\varphi \end{cases} \tag{3}$$

where $\underline{e}_X$, $\underline{e}_Y$, $\underline{e}_Z$ are respectively the unit vectors of the cartesian coordinate system related to the beam axes and $\underline{l}$, $\underline{t}$, $\underline{n}$ are respectively the unit vectors of warp, weft and the normal directions of the local coordinate system related to each point of the membrane according to the principal directions of the fabric. φ is the angle between Z-axis of the beam and the normal of the membrane at the current point. $\varphi = (\underline{e}_Z, \underline{n})$.

We deduce the rotation matrix allowing to pass from the local coordinate system related to the orthotropic directions to the cartesian coordinate system related to the beam:

$$\underline{\underline{R}} = \begin{pmatrix} 1 & 0 & 0 \\ 0 & c & -s \\ 0 & s & c \end{pmatrix} \tag{4}$$

where $c = \cos\varphi$ and $s = \sin\varphi$.

By neglecting the stresses in the normal direction of the fabric (plane stresses hypothesis), the second Piola Kirchhoff tensor can be written in the local $(\underline{l}, \underline{t}, \underline{n})$-axes as:

$$\underline{\underline{S}}^{loc} = \begin{bmatrix} S_{ll} & S_{lt} & 0 \\ S_{lt} & S_{tt} & 0 \\ 0 & 0 & 0 \end{bmatrix} \tag{5}$$

Then, the elasticity tensor expressed in the orthotropic $l-t$ basis is written as:

$$\underline{\underline{\underline{C}}}^{loc} = \begin{bmatrix} C_{11} & C_{12} & 0 \\ C_{12} & C_{22} & 0 \\ 0 & 0 & C_{66} \end{bmatrix} \tag{6}$$

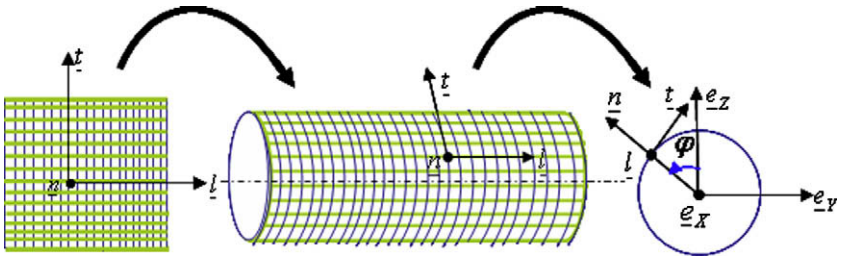

Fig. 2. Definition of warp and weft axes $(\underline{l},\underline{t},\underline{n})$ and beam axes $(\underline{e}_X,\underline{e}_Y,\underline{e}_Z)$.

and the components of $\underline{\underline{\underline{\underline{C}}}}^{loc}$ are given in Apedo et al. (2009) as a function of the mechanical properties of the fabric.

To compute the elasticity tensor expressed in the beam axes, one can use the transformation:

$$C_{ijkl} = R_{im}R_{jn}R_{kp}R_{lq}C^{loc}_{mnpq} \tag{7}$$

The Saint Venant–Kirchhoff hypothesis is often used in the literature (Le Van and Wielgosz, 2005, 2007; Davids and Zhang, 2008) i.e. the components S_{YY}, S_{YZ} and S_{ZZ} of the second Piola Kirchhoff tensor in the beam coordinate system, are not neglected *a priori*. This hypothesis is not used here and then the second Piola Kirchhoff tensor is written in the beam coordinate system as follows:

$$\underline{\underline{S}} = \begin{bmatrix} S_{XX} & S_{XY} & S_{XZ} \\ & S_{YY} & S_{YZ} \\ symmetrical & & S_{ZZ} \end{bmatrix} \tag{8}$$

2.3. Variational formulation

The virtual work principle is formulated in the following way:

$$\delta W_{int} + \delta W_{ext} = 0 \tag{9}$$

where δW_{int} is the internal virtual work and δW_{ext} is the external virtual work. The internal virtual work is formulated as:

$$\delta W_{int} = -\int_{V_o} \underline{\underline{S}} : \delta\underline{\underline{E}}\, dV_o \tag{10}$$

where V_o is the 3D region occupied by the beam in the reference configuration, $\underline{\underline{S}}$ is the second Piola–Kirchhoff tensor by including the effect of the prestressing due to the inflation and $\delta\underline{\underline{E}}$, the virtual Green tensor. One can re-write (10) as:

$$\begin{aligned} -\delta W_{int} = \int_0^{l_o} \{ & [(1+u_{,X})N + M_y\theta_{Y,X} + M_z\theta_{Z,X} - T_y\theta_Z \\ & + T_z\theta_Y]\delta u_{,X} + (Nv_{,X} + T_y)\delta v_{,X} + (Nw_{,X} + T_z)\delta w_{,X} \\ & + [M_y(1+u_{,X}). + Q_1\theta_{Z,X} + Q_2\theta_{Y,X} + Q_3\theta_Z \\ & + Q_4\theta_Y]\delta\theta_{Y,X} + [M_z(1+u_{,X}).. + Q_5\theta_{Z,X} + Q_1\theta_{Y,X} \\ & + Q_6\theta_Z + Q_7\theta_Y]\delta\theta_{Z,X} + [T_z(1+u_{,X}). + Q_4\theta_{Y,X} \\ & + Q_7\theta_{Z,X} + Q_9\theta_Y + Q_{10}\theta_Z]\delta\theta_Y + [-T_y(1+u_{,X}) \\ & + Q_3\theta_{Y,X} + Q_6\theta_{Z,X} + Q_8\theta_Z + Q_{10}\theta_Y]\delta\theta_Z\} dX \end{aligned} \tag{11}$$

where N denotes the axial force and T_y and T_z denote the shear forces in Y and Z directions respectively, while M_y and M_z denote the moments around the Y and Z axes respectively. These generalized resultant forces, moments and quantities Q_i ($i = 1,\ldots,10$) acting over the reference cross-section A_o can be related to the stresses in the beam, as given in Apedo et al. (2009).

The external virtual work is due to the inflation pressure and to the dead loads which may include concentrated loads and moments, as well as distributed loads. The external virtual work due to the dead loads can be written as:

$$\begin{aligned} \delta W^d_{ext} = & \int_0^{l_o} (f_x\delta u + f_y\delta v + f_z\delta w)dX + \sum_{i=1}^{n}[F_X(X_i)\delta u(X_i) \\ & + F_Y(X_i)\delta v(X_i) + F_Z(X_i)\delta w(X_i) + M_Y(X_i)\delta\theta_Y(X_i) \\ & + M_Z(X_i)\delta\theta_Z(X_i)] \end{aligned} \tag{12}$$

In which f_x, f_y and f_z are respectively the distributed loads along X, Y, and Z axes, while $F_a(b)$, and $M_a(b)$ ($a = X,Y,Z$; $b = X_1,\ldots,X_n$) are the external supports reactions and external loads and moments.

The initial pressurization takes place prior to the application of external dead loads. The inflation pressure p is assumed to remain constant. This assumption is consistent with prior studies of inflated fabric beams and arches (Main et al., 1995; Steeves, 1975; Cavallaro et al., 2003; Le Van and Wielgosz, 2005; Davids and Zhang, 2008; Comer and Levy, 1963; Webber, 1982). It is noted that a more rigorous analysis would couple a gas law with the mechanics simulation, allowing the consideration of pressure change with deformation-induced volume changes. This effect has been considered in prior studies (Berry and Yang, 1996; Cavallaro and Sadegh, 2006; Cavallaro et al., 2007). Proceeding like in Le Van and Wielgosz (2005), the external virtual work due to the inflation pressure is found to be:

$$\begin{aligned} \delta W^p_{ext} = & F_p\int_0^{l_o} (v_{,X}\delta\theta_Z - w_{,X}\delta\theta_Y - \theta_{Z,X}\delta v + \theta_{Y,X}\delta w)dX \\ & - F_p[\delta u(0) + \theta_Z(0)\delta v(0) - \theta_Y(0)\delta w(0) - \delta u(l_o) \\ & - \theta_Z(l_o)\delta v(l_o) + \theta_Y(l_o)\delta w(l_o)] \end{aligned} \tag{13}$$

with $F_p = p\Pi R_o^2$. Note also that the reference dimensions l_o, R_o and t_o depend on the inflation pressure and the mechanical properties of the fabric (see Apedo et al., 2009).

One can see that the inflation pressure generates follower forces which induce nonlinear effect when the beam deflects.

3. Finite element implementation

To carry out an approximate solution of the displacements field, the inflatable beam is discretized by the finite element method. The choice of an element for discretizing the equation (9) is then the first step of this implementation. The elements often used for inflatable beams are linear two-noded element for Euler–Bernoulli kinematics with Hermite polynomial as shape functions (Bhatti, 2006), or a higher order element such as the three-noded quadratic beam with reduced integration (Le Van and Wielgosz, 2007) or the three-noded Timoshenko beam that has quadratic shape functions for transverse displacement and linear shape functions for bending rotation and axial displacement (Davids, 2007; Davids and Zhang, 2008). A two-noded mixed interpolation beam element where the shape functions are constrained to satisfy the governing differential equilibrium equations for a Timoshenko beam element, can also be used (Friedman and Kosmatka, 1993). This element has cubic displacement shape functions and does not exhibit shear locking.

In the present analysis, a three-noded Timoshenko beam element is used. The quadratic shape functions are used for all the components of the displacements field (i.e. u, v, w, θ_Y and θ_Z).

3.1. Element description

A three-noded element is used. This element has five degrees of freedom at each node: axial displacement u along the local X-axis of the beam element, two transverse displacements v and w along the two principal axes of inertia of the cross-section and the two bending rotations θ_Y and θ_Z. The element displacements vector U^e for an element is given by (14)

$$U^e = \left[U_1^e \;\; V_1^e \;\; W_1^e \;\; \theta_{Y1}^e \;\; \theta_{Z1}^e \;\; U_2^e \;\; V_2^e \;\; W_2^e \;\; \theta_{Y2}^e \;\; \theta_{Z2}^e \;\; U_3^e \;\; V_3^e \;\; W_3^e \;\; \theta_{Y3}^e \;\; \theta_{Z3}^e\right]^T \tag{14}$$

The components of the displacements field can be expressed as:

$$\begin{Bmatrix} u \\ v \\ w \\ \theta_Y \\ \theta_Z \end{Bmatrix} = \begin{bmatrix} N_u^T \\ N_v^T \\ N_w^T \\ N_{\theta_Y}^T \\ N_{\theta_Z}^T \end{bmatrix} U^e \tag{15}$$

where N_u, N_v, N_w, N_{θ_Y} and N_{θ_Z} are listed in Appendix A.

The virtual displacements $\delta u, \delta v, \delta w, \delta\theta_Y$ and $\delta\theta_Z$ are interpolated in the same way:

$$\begin{Bmatrix} \delta u \\ \delta v \\ \delta w \\ \delta\theta_Y \\ \delta\theta_Z \end{Bmatrix} = \begin{bmatrix} N_u^T \\ N_v^T \\ N_w^T \\ N_{\theta_Y}^T \\ N_{\theta_Z}^T \end{bmatrix} \delta U^e \tag{16}$$

where δU^e is the virtual displacement associated with U^e.

3.2. Discretization and solution

By substituting in the expressions of all the terms derived from the virtual work principle (Eqs. (11)–(13)), the displacements and the virtual displacements expressions presented in Section 3.1, one gets the following expressions in the element level:

$$\delta W_{int}^e = -\int_{V_o^e} \underline{\underline{S}} : \delta\underline{\underline{E}}\, dV_o^e = \delta U^{eT} \int_0^{l_o^e} [G(X)]^T \begin{Bmatrix} A_1(X) \\ B_1(X) \\ C_1(X) \\ D_1(X) \\ E_1(X) \\ F_1(X) \\ H_1(X) \end{Bmatrix} dX \tag{17}$$

where the quantities A_1, B_1, C_1, D_1, E_1, F_1, H_1 and $[G]$ are given in Appendix A.

Then, one can identify the element's internal force vector as:

$$F_{int}^e = \int_0^{l_o^e} [G(X)]^T \begin{Bmatrix} A_1(X) \\ B_1(X) \\ C_1(X) \\ D_1(X) \\ E_1(X) \\ F_1(X) \\ H_1(X) \end{Bmatrix} dX = \frac{l_o^e}{2} \int_{-1}^{1} [G(\xi)]^T \begin{Bmatrix} A_1(\xi) \\ B_1(\xi) \\ C_1(\xi) \\ D_1(\xi) \\ E_1(\xi) \\ F_1(\xi) \\ H_1(\xi) \end{Bmatrix} d\xi \tag{18}$$

The discretization of the external virtual work due to the inflation pressure is given by:

$$\delta W_{ext}^{e^p} = \delta U^{eT} F_{ext}^{e^p} \tag{19}$$

where

$$F_{ext}^{e^p} = F_p \int_0^{l_o^e} [T_1(X)]^T \begin{Bmatrix} 1 \\ \theta_Z \\ -\theta_Y \\ -w_X \\ v_X \end{Bmatrix} dX = F_p \frac{l_o^e}{2} \int_{-1}^{1} [T_1(\xi)]^T \begin{Bmatrix} 1 \\ (\kappa_{\theta_Z} N_{\theta_Z})^T \kappa_{\theta_Z} U^e \\ -(\kappa_{\theta_Y} N_{\theta_Y})^T \kappa_{\theta_Y} U^e \\ -\frac{2}{l_o^e} (\kappa_w N_{w,\xi})^T \kappa_w U^e \\ \frac{2}{l_o^e} (\kappa_v N_{v,\xi})^T \kappa_v U^e \end{Bmatrix} d\xi \tag{20}$$

and $[T_1]$ is given in Appendix A.

One can note according to (20), the follower force effect of the external load due to the inflation pressure.

The discretization of the external virtual work due to the dead load is given by:

$$\delta W_{ext}^{e^d} = \delta U^{eT} F_{ext}^{e^d} \tag{21}$$

where

$$F_{ext}^{e^d} = F^e + \int_0^{l_o^e} [T_2(X)]^T \begin{Bmatrix} f_x \\ f_y \\ f_z \\ 0 \\ 0 \end{Bmatrix} dX = F^e + \frac{l_o^e}{2} \int_{-1}^{1} [T_2(\xi)]^T \begin{Bmatrix} f_x \\ f_y \\ f_z \\ 0 \\ 0 \end{Bmatrix} d\xi \tag{22}$$

$[T_2]$ and F^e are given in Appendix A.

The discretized virtual work principle is then given by:

$$\delta W_{int}^e + \delta W_{ext}^e = \delta U^{eT} \Re^e = 0 \tag{23}$$

with

$$\delta W_{ext}^e = \delta W_{ext}^{e^p} + \delta W_{ext}^{e^d} \tag{24}$$

As δU^e is a vector of arbitrary virtual nodal displacements, Eq. (23), leads to:

$$\Re^e = F_{ext}^{e^d} + F_{ext}^{e^p} - F_{int}^e = F_{ext}^e - F_{int}^e = F_{ext}^e - [K^e]U^e = 0 \tag{25}$$

where $\Re^e$ is the unbalanced residual force vector of the element "e" and K^e is the element stiffness matrix. As the problem is nonlinear,the stiffness matrix can be written as:

$$[K^e] = \left[K_E^e\right] + \left[K_G^e(U^e)\right] \tag{26}$$

where $\left[K_E^e\right]$ is the elastic stiffness matrix calculated for the element geometry at the start of the step and $\left[K_G^e(U^e)\right]$ is the so-called geometrical stiffness matrix, which depends not only on the geometry but also on the initial internal stresses existing at the start of the step.

To solve (25), an iterative scheme is often used. This scheme will be detailed in Section 3.2.2. One defines the tangent stiffness matrix of the element "e" as:

$$\begin{aligned} \left[K_T^e\right] &= -\frac{\partial \Re^e}{\partial U^e} = -\frac{\partial F_{ext}^{e^p}}{\partial U^e} + \frac{\partial [K_G^e(U^e)]}{\partial U^e} U^e + [K^e] \\ &= \int_0^{l_o^e} [G(X)]^T ([\Omega_{int}(X)] - [\Omega_{ext}])[G(X)] dX \\ &= \frac{l_o^e}{2} \int_{-1}^{1} [G(\xi)]^T ([\Omega_{int}(\xi)] - [\Omega_{ext}])[G(\xi)] d\xi \end{aligned} \tag{27}$$

where $[\Omega_{int}]$ and $[\Omega_{ext}]$ are given in Appendix A.

As in the case of (26), the tangent stiffness matrix can also be written as:

$$\left[K_T^e\right] = \left[K_{ET}^e\right] + \left[K_{GT}^e\right] \tag{28}$$

in which, only $\left[K_{GT}^e\right]$ is a function of U^e. In the following sections, two kinds of solutions of inflatable beams are investigated.

3.2.1. Linear finite element solution for inflatable beams

To obtain the linear finite element model, $[K_T^e]$ is generally assumed not to be a function of U^e (Le Van and Wielgosz, 2007), hence the entries of the matrix $[K_{GT}^e(U^e)]$ are equal to zeros. Consequently, the inflatable beam response evolves linearly when applying the dead loads. In this case, $[K_T^e]$ can be reduced to:

$$\begin{aligned}[K_T^e] &= [K_{ET}^e] = -\left.\frac{\partial F_{ext}^{ep}}{\partial U^e}\right|_{U^e=0} + [K_E^e] \\ &= \int_0^{l_o^e} [G(X)]^T([\Omega_{intLin}] - [\Omega_{ext}])[G(X)]dX \\ &= \frac{l_o^e}{2}\int_{-1}^{1} [G(\xi)]^T([\Omega_{intLin}] - [\Omega_{ext}])[G(\xi)]d\xi \end{aligned} \tag{29}$$

where

$$[\Omega_{intLin}] = \begin{bmatrix} N^o + C_{11}A_o & 0 & 0 & 0 & 0 & 0 & 0 \\ & N^o + C_y & 0 & 0 & 0 & -C_y & 0 \\ & & N^o + C_z & C_z & 0 & 0 & 0 \\ & & & N^o + C_z & 0 & 0 & 0 \\ & & & & \left(\frac{N^o}{A_o} + C_{11}\right)I_o & 0 & 0 \\ & & & & & N^o + C_y & 0 \\ symmetric & & & & & & \left(\frac{N^o}{A_o} + C_{11}\right)I_o \end{bmatrix} \tag{30}$$

where $C_y = \frac{1}{2}k_yA_oC_{66}$ and $C_z = \frac{1}{2}k_zA_oC_{66}$

So, for a linear finite element inflatable beam, the displacements field can be obtained from:

$$[K_{ET}^e]U^e = F_{ext}^{ed} \tag{31}$$

The components of the stiffness matrix $[K_{ET}^e]$ in the case of a three-noded Timoshenko beam element with full integration over all the terms, are given in Appendix B. One can note that, after this linearization, only the Young modulus in the warp direction (direction coinciding with the beam axis) and the in-plane shear modulus intervene explicitly in the stiffness matrix (through C_{11} and C_{66}). In addition, one can notice that the Young modulus in the weft direction of the fabric also appears but only through the dimensions of the beam in the prestressed reference configuration (Apedo et al., 2009).

The structural equilibrium equations are obtained by assembling over the all model, the local equilibrium equations and one obtains

$$[K_{ET}]U = F_{ext}^d \tag{32}$$

where $[K_{ET}]$ is the global elastic stiffness matrix, U is the global nodal displacements vector and F_{ext}^d, the global nodal dead load vector. To simplify in the following, $[K_{ET}]$ will be noted by $[K]$.

3.2.2. Nonlinear finite element solution for inflatable beams

The nonlinear equilibrium equation (25) for a given element, is reformulated in

$$[K_T^e]\Delta U^e = \Re^e \tag{33}$$

in which $[K_T^e]$ is the element tangent stiffness matrix including the inflation pressure effect and still given by (27), $\Re^e$ is the element unbalanced residual force vector and ΔU^e is an unknown displacement increment to be solved for. After assembling (33) over all the elements in the model, the following equilibrium equation is obtained

$$[K_T]\Delta U = \Re \tag{34}$$

where $[K_T]$, ΔU and $\Re$ are respectively, the global tangent stiffness matrix, the global requested displacement increment and the global unbalanced residual force vector. The procedure was implemented using the scientific and engineering computing package MATLAB. An iterative scheme based on the Quasi-Newton, is used to solve Eq. (34). The beam is discretized in several 3-noded finite elements and each node has 5 degrees of freedom. For each element with number "e", the unbalanced residual force vector $\Re^e$ is evaluated. After assembling, the numerical problem to be solved at the iteration i is:

$$[K_T]\Delta U^i = \Re(U^{i-1}) = \Re^i \tag{35}$$

where $\Re^i$ is the global unbalanced residual force vector from the previous iteration and $\Delta U^i = U^i - U^{i-1}$, is the unknown displacement increment at iteration i with U^{i-1}, the known global nodal displacements vector of the previous solution step and U^i, the unknown global nodal displacements vector to be solved for. The termination criterion is given by (36).

$$\|\Delta U^i\| = [(\Delta U^i)^T\Delta U^i]^{\frac{1}{2}} \leqslant 10^{-6} \quad \text{or} \quad \|\Re^i\| = [(\Re^i)^T\Re^i]^{\frac{1}{2}} \leqslant 10^{-6} \tag{36}$$

4. Validation

To validate the beam models presented in the previous sections of this paper, a reference model is provided. As the beam is made from fabric, the beam theories used here are meaningful only if one can compare them to a thin-shell model (Plaut et al., 2000; Molloy, 1998; Molloy et al., 1999; Veldman et al., 2005) or a membrane 3D model (Wielgosz and Thomas, 2002, 2003; Le Van and Wielgosz, 2005, 2007). For Veldman et al. (2005), the right choice of a model depends on the range of the inflation pressures. They have proposed to model the beam as a thin shell instead of a membrane 3D for pressures around 25 kPa. This approach is adopted here and a thin-shell model is chosen as the reference model because this type of element is less time consuming than the membrane element, for about the same results. Then, the nonlinear beam finite element model is compared to the reference model. The in-plane bending problem of an inflatable cantilever beam is investigated. The beam is built-in at end $X = 0$, subjected to an internal pressure p. An external load F is applied at the end $X = l_o$ (Fig. 3). Following the normalization procedure proposed in Houliara and Karamanos (2006, 2010), the values of pressure p and load F are normalized by $p_{cr} = \frac{E_l t_\phi^3}{4R_\phi^3(1-\nu_{lt}\nu_{tl})}$ and $F_e = \frac{E_t R_\phi t_\phi^3}{q l_\phi \sqrt{1-\nu_{lt}\nu_{tl}}}$, respectively; the normalized variables are: $p_n = \frac{p}{p_{cr}}$, $f = \frac{F}{F_e}$, $q = \sqrt{\frac{E_t}{E_l}}$ is a parameter indicating the level of anisotropy. Bending deflection is normalized by the cylinder's natural radius R_ϕ.

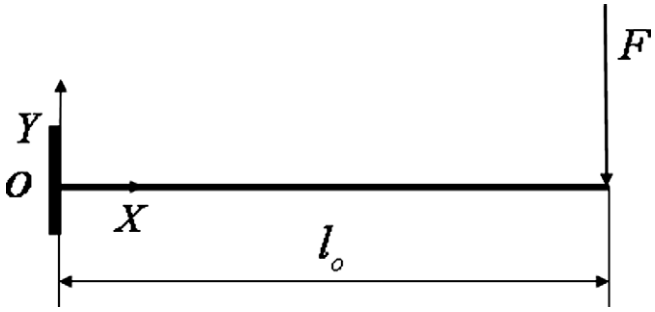

Fig. 3. Cantilever beam under concentrated load.

4.1. Reference model: numerical thin-shell simulations

ABAQUS/Standard is chosen as the FEA package for this purpose, based primarily on its robust nonlinear solver. General purpose three-noded and four-noded thin-shell elements generated automatically, are used to model the beam. As an example, the bending problem of a cantilever beam under concentrated load, is considered. All the end surface $X = 0$ is built-in. A mesh refinement study is conducted to determine a reasonable element density. Uniform meshes of the cylindrical beams are created with varying average element sizes from 10 mm to 40 mm. The cantilever beam model is run at several inflation pressures and the concentrated loads used are 20*N* and 200*N*. At every pressure, the deflection is recorded for several average element sizes. The density meshes of 30 mm is finally adopted because it allows a good convergence. This mesh has 2862 elements (2850 linear quadrilateral elements of type S4R and 12 linear triangular elements of type S3) and 2858 nodes, (see Fig. 4). The geometrical properties of the beam are taken from Table 1. The nonlinear geometrical effects are included into the analysis which is performed in two steps. At the first step, the inflation pressure is applied to both the lateral and end surfaces of the beam, and at the second step, the external dead load is applied. As only a static analysis is performed, the model does not take into account the fluid solid interaction. This assumption is already adopted by many authors (Steeves, 1975; Le Van and Wielgosz, 2005; Fichter, 1966; Davids and Zhang, 2008). A linearly elastic orthotropic laminate material termed "LAMINA" in ABAQUS, is used. This type of material allows the user to directly input two orthotropic elastic moduli (E_l and E_t), the in-plane shear modulus (G_{lt}) and the in-plane Poisson's ratio (ν_{lt}). To show the influence of the mechanical properties on the beam response, two fabrics previously used in the literature (Apedo et al., 2009; Vysochina, 2005; Cheng and Xiong, 2009) are tested. The first has lower mechanical properties (case 1) than the second (case 2). One can see Table 1 for more details.

Table 1
Data for inflatable beam.

Natural thickness, $t_\phi(m)$		10^{-3}
Shear correction coefficient, k_y		0.5
Natural radius, $R_\phi(m)$		0.14
Natural length, $l_\phi(m)$		3
Mechanical properties		
	Case 1	Case 2
Young modulus in warp direction, E_l (MPa)	393.13	18370
Young modulus in weft direction, E_t (MPa)	451.59	14120
In-plane shear modulus, G_{lt} (MPa)	103	6460
Poisson ratio, ν_{lt}	0.07	0.28
Poisson ratio, ν_{tl}	0.08	0.22

The pressure values and the associated normalized pressure are listed in Table 2.

4.2. Linear finite element model

The linear beam finite element developed in Section 3.2.1 is used to obtain the deflection. However, a Timoshenko beam element must be used, a shear locking problem is arised when a full integration is performed. To avoid this coupling between bending and shear effects, one can perform a reduced integration of the terms $N^T_{\theta_Y}N_{\theta_Y}$, $N^T_{\theta_Y}N_{\theta_Z}$, $N^T_{\theta_Z}N_{\theta_Y}$ and $N^T_{\theta_Z}N_{\theta_Z}$ with two Gauss integration points $\xi = \frac{\pm 1}{\sqrt{3}}$. With this reduced integration, the components of the stiffness matrix remain the same with the exception of the components listed in Appendix B. If only one element is considered

Table 2
Normalized pressure (p_n) for different values of pressure (p) used in the paper.

p (kPa)	p_n	
	Material case 1	Material case 2
10	278	6
20	555	11
25	694	14
30	833	17
40	1111	22
50	1388	28
100	2776	56
150	4164	84
200	5553	112
250	6941	140

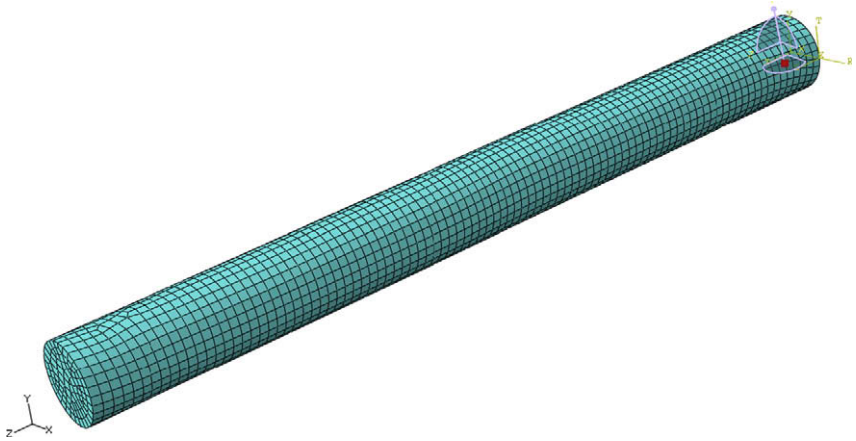

Fig. 4. The beam mesh.

to describe the beam, by solving the problem formulated in (32) with the boundary conditions ($V_1 = \theta_{Z1} = 0$), one obtains the following nodal deflections and rotations when a reduced integration is performed:

$$V_2 = \frac{5Fl_o^3}{48\left(C_{11} + \frac{F_p}{A_o}\right)I_o} + \frac{Fl_o}{2\left(F_p + \frac{1}{2}k_y A_o C_{66}\right)}, \quad \theta_{Z2} = \frac{3Fl_o^2}{8(C_{11} + \frac{F_p}{A_o})I_o} \tag{37a}$$

$$V_3 = \frac{Fl_o^3}{3\left(C_{11} + \frac{F_p}{A_o}\right)I_o} + \frac{Fl_o}{F_p + \frac{1}{2}k_y A_o C_{66}}, \quad \theta_{Z3} = \frac{Fl_o^2}{2\left(C_{11} + \frac{F_p}{A_o}\right)I_o} \tag{37b}$$

These results are close to the analytical solutions proposed in Apedo et al. (2009)

The inflatable beam is discretized in several finite elements. A mesh refinement study is conducted to determine a reasonable element density. Figs. 5 and 6 show the results for both cases of mechanical properties. Finally, 50 elements are used to discretize the beam.

Figs. 7 and 8 show the evolution of the normalized maximum deflection as a function of the normalized applied load in the linear finite element model case. In the case 1 (Fig. 7), the influence of the inflation pressure is noticeable whereas, in the case 2 (Fig. 8), the inflation pressure does not influence enough the deflection. Whatever the type of material, the curves obtained are obviously linear.

4.3. Nonlinear finite element model

The inflatable cantilever beam is investigated by the nonlinear procedure proposed in Section 3.2.2. The three-noded quadratic elements are used. A mesh refinement study is conducted to determine a reasonable number of elements to use for insure the convergence. Figs. 9 and 10 show the results in both cases of mechanical properties. One can notice that, 50 quadratic elements are sufficient to ensure convergence.

Figs. 11 and 12 correspond to the graphs of the normalized maximum deflection versus the normalized load. In case 1 (Fig. 11), one can notice that the curves are nonlinear for each pressure and the effect of the pressure on the beam behaviour is significant, on the other hand, the effect of the pressure is not noticeable in the material case 2 (Fig. 12).

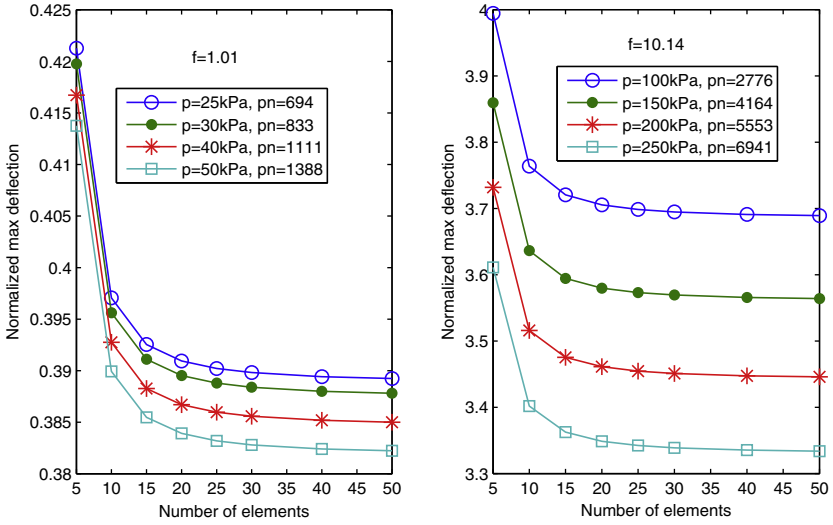

Fig. 5. Linear finite element model: results of the influence of the number of elements in case 1.

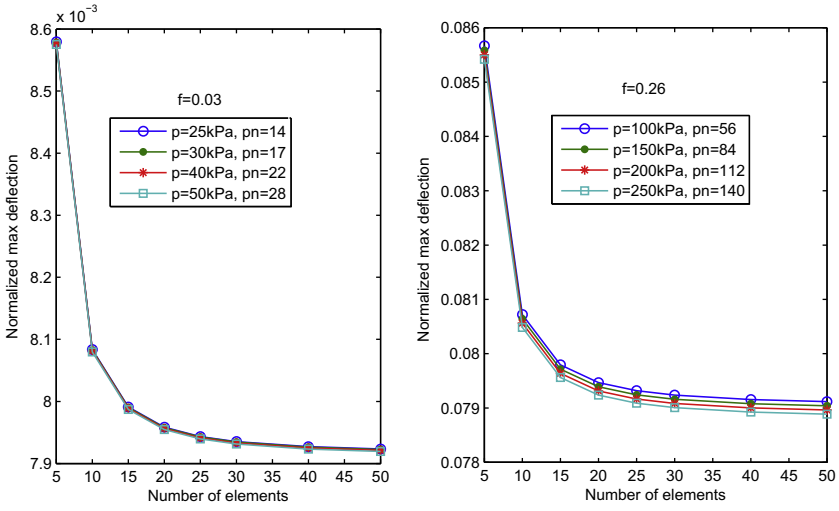

Fig. 6. Linear finite element model: results of the influence of the number of elements in case 2.

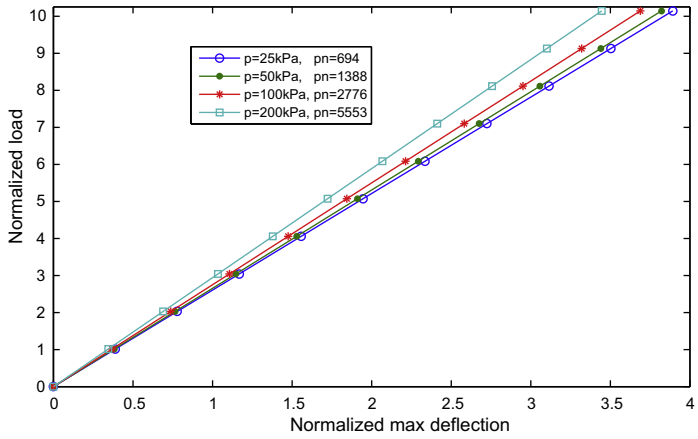

Fig. 7. Linear finite element model: load–maximum deflection in case 1.

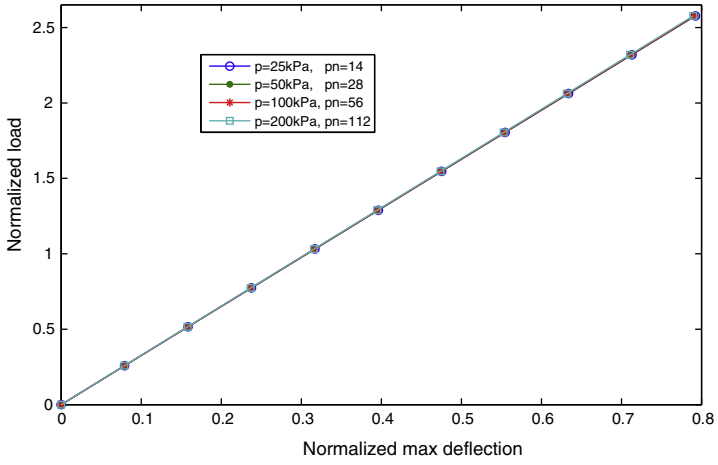

Fig. 8. Linear finite element model: load–maximum deflection in case 2.

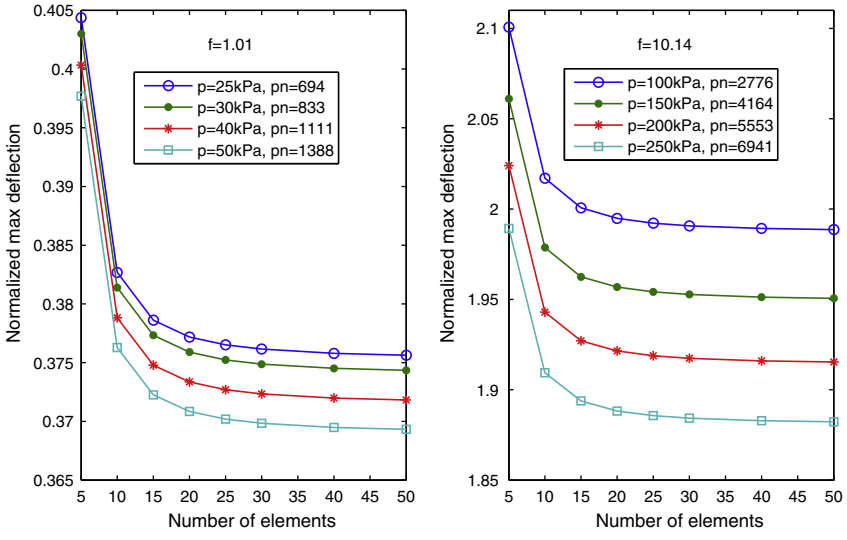

Fig. 9. Nonlinear finite element model: results of the influence of the number of elements in case 1.

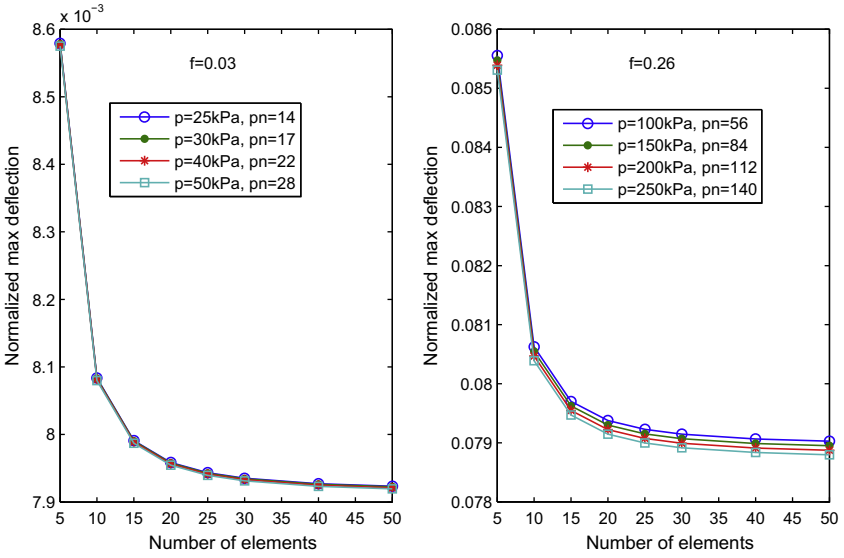

Fig. 10. Nonlinear finite element model: results of the influence of the number of elements in case 2.

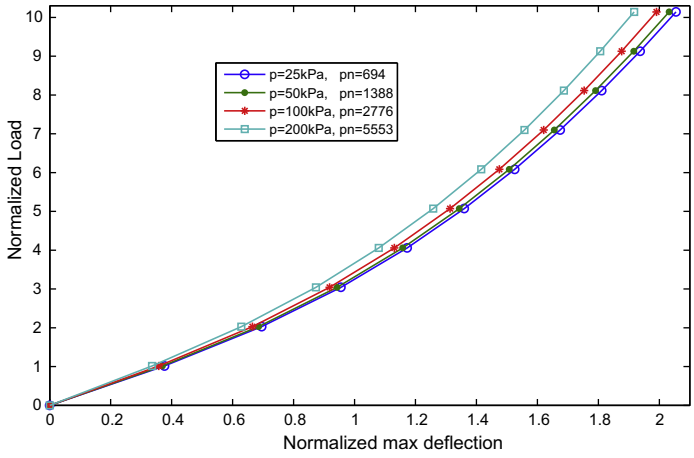

Fig. 11. Nonlinear finite element model: load–maximum deflection in case 1.

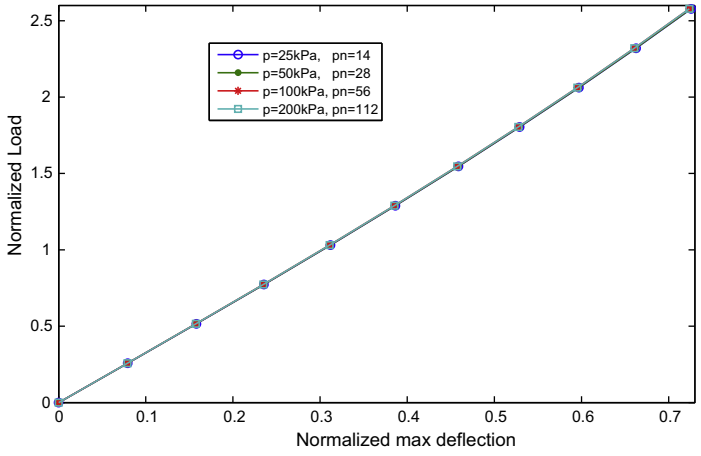

Fig. 12. Nonlinear finite element model: load–maximum deflection in case 2.

4.4. Validation of the nonlinear beam finite element (FE) model and analysis

4.4.1. Validation of the nonlinear beam finite element model

In this section, a comparison is performed between the nonlinear FE beam model and the nonlinear thin-shell model (the reference model). The values given in Table 3 are obtained from the simulations with both given in Table 1.

In case 1, in the reference model, a convergence problem is encountered for high pressures and for high died loads: this convergence problem is due to local instabilities. So, one loading case ($F = 20N$ corresponding to $f = 1.01$ for the material case 1) is treated and the pressures used are relatively low. The maximum error is 2.6% between the reference model and the nonlinear beam finite element model (see Table 3).

Note that, the beam theories developed here are valid only when local instabilities (wrinkling) do not appear. Several theories exist on the prediction of the wrinkling appearance (see Le Van and Wielgosz, 2005; Apedo et al., 2009; Main et al., 1995; Veldman et al., 2005 for example). Apedo et al. (2009) have recently proposed an expression for the wrinkling load:

$$F_w = \frac{\pi R_o^3 p}{2 l_o}\left(1 + \frac{p R_o}{2 C_{11} t_o}\right) \tag{38}$$

Fig. 13 shows the evolution of the normalized wrinkling load as function of the normalized inflation pressure for case 1. In case 2, no instability occurs for the pressure and the load applied. Two loads cases are treated. The maximum error between the reference model and the nonlinear beam finite element is 5.95% (see Table 3).

These various results show that the model FE beam nonlinear is appropriate to model the inflatable beams whatever the mechanical properties of fabric when no strong instability occurs (limit of the model).

4.4.2. Analysis of beam models

In this section, the linear beam finite element model is compared to the nonlinear beam finite element model. Two cases of bending loads are investigated (20*N* and 200*N*, corresponding to

Table 3
Comparison between maximum deflections of the nonlinear beam FE (NLBFE) and the nonlinear Shell FE (NLSFE) model.

Load (N)	Normalized load	Material	Normalized pressure	Normalized max deflection $X\ 10^3$		Error (%)
				NLSFE model	NLBFE model	
20	1.01	Case 1	278	380.714	379.286	0.38
			555	372.857	377.143	1.15
			694	368.571	375.714	1.94
			833	365.714	374.286	2.34
			1111	364.286	372.143	2.16
			1388	360.000	369.286	2.58
200	0.03	Case 2	14	8.164	7.924	2.94
			17	8.143	7.923	2.70
			22	8.095	7.923	2.13
			28	8.054	7.919	1.68
			56	7.875	7.911	0.46
			84	7.719	7.904	2.40
			112	7.578	7.896	4.20
			140	7.446	7.889	5.95
200	0.26	Case 2	14	81.922	79.144	3.39
			17	81.705	79.136	3.14
			22	81.296	79.121	2.68
			28	80.912	79.106	2.23
			56	79.237	79.029	0.26
			84	77.815	78.952	1.15
			112	76.556	78.876	3.03
			140	75.414	78.799	4.49

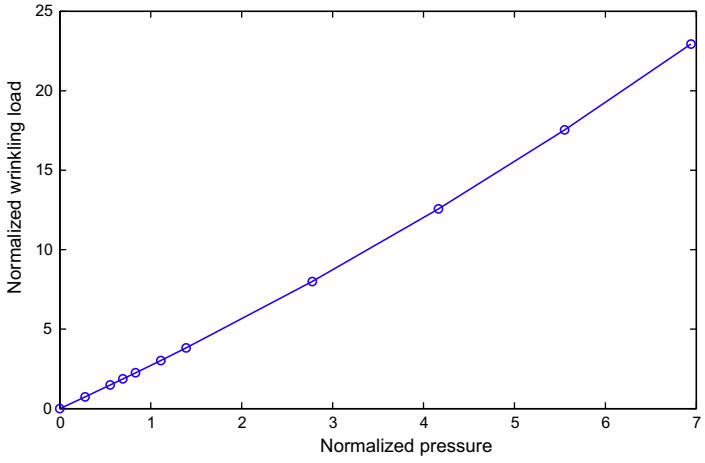

Fig. 13. Wrinkling load.

Table 4
Comparison between maximum deflections of the linear (LBFE) and the nonlinear (NLBFE) beam FE models.

Load (N)	Normalized load	Material	Normalized pressure	Normalized max deflection $X\ 10^3$		Discrepancy (%)
				NLBFE model	LBFE model	
20	1.01	Case 1	694	376.156	389.239	3.48
			833	374.351	387.817	3.60
			1111	371.818	385.004	3.55
			1388	369.318	382.229	3.50
			2776	357.782	368.911	3.11
			4164.475	345.911	356.396	3.03
			5553	335.607	344.581	2.67
			6941	324.854	333.379	2.62
20	0.03	Case 2	14	7.924	7.924	0
			17	7.923	7.923	0
			22	7.921	7.921	0
			28	7.919	7.919	0
			56	7.912	7.912	0
			84	7.904	7.904	0
			112	7.896	7.896	0
			140	7.889	7.889	0
200	10.14	Case 1	694	2054.700	3892.386	89.44
			833	2049.079	3878.171	89.26
			1111	2038.900	3850.043	88.83
			1388	2032.229	3822.286	88.08
			2776	1990.729	3689.107	85.31
			4164	1950.600	3563.964	82.71
			5553	1917.414	3445.807	79.71
			6941	1882.229	3333.786	77.12
200	0.26	Case 2	14	79.143	79.236	0.12
			17	79.136	79.223	0.11
			22	79.121	79.214	0.12
			28	79.107	79.193	0.11
			56	79.029	79.121	0.12
			84	78.950	79.043	0.12
			112	78.879	78.964	0.11
			140	78.800	78.886	0.11

f = 1.01 and 10.14 in the material case 1 and f = 0.03 and 0.26 in the material case 2) with both materials as in Sections 4.2 and 4.3.

Table 4 shows the normalized deflection values obtained for both models.

One can observe that with the high mechanical properties, the results of the linearized model coincide almost with those of the nonlinear model FE. In the case of this study, the maximum discrepancy does not reach 0.2% (see Table 4). Thus, it is not necessary to study the inflatable beams with a nonlinear model. A linearized study is appropriate perfectly, even at high and very high pressures. This remark is foreseeable through Figs. 8 and 12. It is the kind of studies that have made Le Van and Wielgosz (2005, 2007)) who have worked on the beams made from isotropic fabric with high mechanical properties and highly inflated. Let us note that the influence of the inflation pressure is not significant in this case (see Fig. 12) and the curves obtained are almost linear.

However, it is not legitimate to be limited only to the linearized study when the properties of material are low, even at low pressures. The geometrical nonlinearities appear rapidly during the loading (see Fig. 11). One can see in Fig. 11 that, the nonlinearities appear when an approximate load of 20N (corresponding to f = 1.01) is applied. For normalized loads lower than 1.01, both models are quite equivalent. On the hand, if an external normalized load higher than 1.01 is applied, both models become dramatically different. In the present study, the maximum discrepancy exceeds 75 % (see Table 4). Therefore, while substituting the nonlinear model by the linear one, the errors which can result, can be dramatic (see Table 4).

5. Summary and conclusion

This paper was devoted to the numerical modelling of inflatable OWF beams. The total Lagrangian form of the virtual work principle and the Timoshenko beam were used to obtain the nonlinear equilibrium equations. The geometrical nonlinearities and the inflation pressure follower force effect were taken into account. Then, the equations were discretized by the finite element method. Two kinds of solutions were proposed: finite element model for linearized problems and nonlinear finite element model. As an example, the bending problem of a cantilever inflatable beam under concentrated load was considered. Inflatable beams with different mechanical properties were studied. The beam models were shown to be in a good agreement with the nonlinear thin-shell model. So, these beam models are very interesting because they give almost the same results as the reference model although they use nearly 300 times less degrees of freedom than the reference model. This good agreement between the beam finite element and the thin-shell models indicates that the beam models will be useful for the design of inflatable OWF beams and arches when the wrinkles are not yet appear. The results showed also that inflatable beams with low mechanical properties cannot be modelled with the linearized finite elements model because the discrepancy between this model and the nonlinear model can be very high especially when the external load is very high. On the other hand, the linearized model is sufficient to model inflatable beams when the fabric's mechanical properties are high. One can note that for

this kind of material, the inflation pressure does not influence so much the deflection results.

The forthcoming study will study the improvement of the model by taking into account the wrinkling, the cross section ovalization and the fabric failure detections as done in Harursampath and Hodges (1999) and Houliara and Karamanos (2006, 2010).

Also, with the models presented here, ongoing research will be developed to investigate the shape optimization studies of inflatable beams and arches in Civil Engineering constructions.

Acknowledgements

The authors thank LOSBERGER company and specially the Technical Director Mr. Robert Dartois for their useful collaboration.

Appendix A. Internal forces in discretized form, the shape functions and other quantities used in the discretization

$$N = N^o + \frac{2}{l_o^e} C_{11} A_o \left\{ (\kappa_u N_{u,\xi})^T \kappa_u U^e + \frac{1}{l_o^e} [((\kappa_u N_{u,\xi})^T \kappa_u U^e)^2 + ((\kappa_v N_{v,\xi})^T \kappa_v U^e)^2 + ((\kappa_w N_{w,\xi})^T \kappa_w U^e)^2] \right\} + \frac{2}{l_o^{e^2}} C_{11} I_o [((\kappa_{\theta_Y} N_{\theta_Y,\xi})^T \kappa_{\theta_Y} U^e)^2 + ((\kappa_{\theta_Z} N_{\theta_Z,\xi})^T \kappa_{\theta_Z} U^e)^2] + \frac{1}{4} C_{12} A_o [((\kappa_{\theta_Y} N_{\theta_Y})^T \kappa_{\theta_Y} U^e)^2 + ((\kappa_{\theta_Z} N_{\theta_Z})^T \kappa_{\theta_Z} U^e)^2]$$

$$T_y = \frac{1}{2} k_y A_o C_{66} \left[\frac{2}{l_o^e} (\kappa_v N_{v,\xi})^T \kappa_v U^e - (\kappa_{\theta_Z} N_{\theta_Z})^T \kappa_{\theta_Z} U^e (1 + \frac{2}{l_o^e} (\kappa_u N_{u,\xi})^T \kappa_u U^e) \right]$$

$$T_z = \frac{1}{2} k_z A_o C_{66} \left[\frac{2}{l_o^e} (\kappa_w N_{w,\xi})^T \kappa_w U^e + (\kappa_{\theta_Y} N_{\theta_Y})^T \kappa_{\theta_Y} U^e (1 + \frac{2}{l_o^e} (\kappa_u N_{u,\xi})^T \kappa_u U^e) \right]$$

$$M_y = \frac{2}{l_o^e} C_{11} I_o (\kappa_{\theta_Y} N_{\theta_Y,\xi})^T \kappa_{\theta_Y} U^e \left[1 + \frac{2}{l_o^e} (\kappa_u N_{u,\xi})^T \kappa_u U^e \right]$$

$$M_z = \frac{2}{l_o^e} C_{11} I_o (\kappa_{\theta_Z} N_{\theta_Z,\xi})^T \kappa_{\theta_Z} U^e \left[1 + \frac{2}{l_o^e} (\kappa_u N_{u,\xi})^T \kappa_u U^e \right]$$

$$Q_1 = \left(\frac{R_o}{l_o^e} \right)^2 C_{11} I_o ((\kappa_{\theta_Y} N_{\theta_Y,\xi})^T \kappa_{\theta_Y} U^e)((\kappa_{\theta_Z} N_{\theta_Z,\xi})^T \kappa_{\theta_Z} U^e) - \frac{1}{4} C_{12} I_o ((\kappa_{\theta_Y} N_{\theta_Y})^T \kappa_{\theta_Y} U^e)((\kappa_{\theta_Z} N_{\theta_Z})^T \kappa_{\theta_Z} U^e)$$

$$Q_2 = I_o \left\{ \frac{N^o}{A_o} + \frac{2}{l_o^e} C_{11} \left[(\kappa_u N_{u,\xi})^T \kappa_u U^e + \frac{1}{l_o^e} (((\kappa_u N_{u,\xi})^T \kappa_u U^e)^2 + ((\kappa_v N_{v,\xi})^T \kappa_v U^e)^2 + ((\kappa_w N_{w,\xi})^T \kappa_w U^e)^2) + \frac{R_o^2}{4 l_o^e} (3((\kappa_{\theta_Y} N_{\theta_Y,\xi})^T \kappa_{\theta_Y} U^e)^2 + ((\kappa_{\theta_Z} N_{\theta_Z,\xi})^T \kappa_{\theta_Z} U^e)^2) \right] + \frac{1}{8} C_{12} [3((\kappa_{\theta_Z} N_{\theta_Z})^T \kappa_{\theta_Z} U^e)^2 + ((\kappa_{\theta_Y} N_{\theta_Y})^T \kappa_{\theta_Y} U^e)^2] \right\}$$

$$Q_3 = \frac{1}{2 l_o^e} C_{66} I_o [3((\kappa_{\theta_Z} N_{\theta_Z})^T \kappa_{\theta_Z} U^e)((\kappa_{\theta_Y} N_{\theta_Y,\xi})^T \kappa_{\theta_Y} U^e) - ((\kappa_{\theta_Y} N_{\theta_Y})^T \kappa_{\theta_Y} U^e)((\kappa_{\theta_Z} N_{\theta_Z,\xi})^T \kappa_{\theta_Z} U^e)]$$

$$Q_4 = \frac{1}{2 l_o^e} C_{66} I_o [((\kappa_{\theta_Y} N_{\theta_Y})^T \kappa_{\theta_Y} U^e)((\kappa_{\theta_Y} N_{\theta_Y,\xi})^T \kappa_{\theta_Y} U^e) - ((\kappa_{\theta_Z} N_{\theta_Z})^T \kappa_{\theta_Z} U^e)((\kappa_{\theta_Z} N_{\theta_Z,\xi})^T \kappa_{\theta_Z} U^e)]$$

$$Q_5 = I_o \left\{ \frac{N^o}{A_o} + \frac{2}{l_o^e} C_{11} \left[(\kappa_u N_{u,\xi})^T \kappa_u U^e + \frac{1}{l_o^e} (((\kappa_u N_{u,\xi})^T \kappa_u U^e)^2 + ((\kappa_v N_{v,\xi})^T \kappa_v U^e)^2 + ((\kappa_w N_{w,\xi})^T \kappa_w U^e)^2) + \frac{R_o^2}{4 l_o^e} (((\kappa_{\theta_Y} N_{\theta_Y,\xi})^T \kappa_{\theta_Y} U^e)^2 + 3((\kappa_{\theta_Z} N_{\theta_Z,\xi})^T \kappa_{\theta_Z} U^e)^2) \right] + \frac{1}{8} C_{12} [((\kappa_{\theta_Z} N_{\theta_Z})^T \kappa_{\theta_Z} U^e)^2 + 3((\kappa_{\theta_Y} N_{\theta_Y})^T \kappa_{\theta_Y} U^e)^2] \right\}$$

$$Q_6 = \frac{1}{2 l_o^e} C_{66} I_o [((\kappa_{\theta_Z} N_{\theta_Z})^T \kappa_{\theta_Z} U^e)((\kappa_{\theta_Z} N_{\theta_Z,\xi})^T \kappa_{\theta_Z} U^e) - ((\kappa_{\theta_Y} N_{\theta_Y})^T \kappa_{\theta_Y} U^e)((\kappa_{\theta_Y} N_{\theta_Y,\xi})^T \kappa_{\theta_Y} U^e)]$$

$$Q_7 = \frac{1}{2 l_o^e} C_{66} I_o [3((\kappa_{\theta_Y} N_{\theta_Y})^T \kappa_{\theta_Y} U^e)((\kappa_{\theta_Z} N_{\theta_Z,\xi})^T \kappa_{\theta_Z} U^e) - ((\kappa_{\theta_Z} N_{\theta_Z})^T \kappa_{\theta_Z} U^e)((\kappa_{\theta_Y} N_{\theta_Y,\xi})^T \kappa_{\theta_Y} U^e)]$$

$$Q_8 = N^o + A_o \left\{ \frac{1}{l_o^e} C_{12} [(\kappa_u N_{u,\xi})^T \kappa_u U^e + \frac{1}{l_o^e} (((\kappa_u N_{u,\xi})^T \kappa_u U^e)^2 + ((\kappa_v N_{v,\xi})^T \kappa_v U^e)^2 + ((\kappa_w N_{w,\xi})^T \kappa_w U^e)^2)] + \frac{1}{16} C_{22} [3((\kappa_{\theta_Z} N_{\theta_Z})^T \kappa_{\theta_Z} U^e)^2 + ((\kappa_{\theta_Y} N_{\theta_Y})^T \kappa_{\theta_Y} U^e)^2] \right\} + \frac{1}{2 l_o^{e^2}} C_{12} I_o [3((\kappa_{\theta_Y} N_{\theta_Y,\xi})^T \kappa_{\theta_Y} U^e)^2 + ((\kappa_{\theta_Z} N_{\theta_Z,\xi})^T \kappa_{\theta_Z} U^e)^2]$$

$$Q_9 = N^o + A_o \left\{ \frac{1}{l_o^e} C_{12} \left[(\kappa_u N_{u,\xi})^T \kappa_u U^e + \frac{1}{l_o^e} (((\kappa_u N_{u,\xi})^T \kappa_u U^e)^2 + ((\kappa_v N_{v,\xi})^T \kappa_v U^e)^2 + ((\kappa_w N_{w,\xi})^T \kappa_w U^e)^2) \right] + \frac{1}{16} C_{22} [3((\kappa_{\theta_Y} N_{\theta_Y})^T \kappa_{\theta_Y} U^e)^2 + ((\kappa_{\theta_Z} N_{\theta_Z})^T \kappa_{\theta_Z} U^e)^2] \right\} + \frac{1}{2 l_o^{e^2}} C_{12} I_o [3((\kappa_{\theta_Z} N_{\theta_Z,\xi})^T \kappa_{\theta_Z} U^e)^2 + ((\kappa_{\theta_Y} N_{\theta_Y,\xi})^T \kappa_{\theta_Y} U^e)^2]$$

$$Q_{10} = \frac{1}{8} C_{22} A_o (((\kappa_{\theta_Y} N_{\theta_Y})^T \kappa_{\theta_Y} U^e)((\kappa_{\theta_Z} N_{\theta_Z})^T \kappa_{\theta_Z} U^e)) - \frac{1}{l_o^{e^2}} C_{12} I_o (((\kappa_{\theta_Y} N_{\theta_Y,\xi})^T \kappa_{\theta_Y} U^e)((\kappa_{\theta_Z} N_{\theta_Z,\xi})^T \kappa_{\theta_Z} U^e))$$

Quantities used in the expression of the discretized virtual works

$$\begin{Bmatrix} A_1(X) \\ B_1(X) \\ C_1(X) \\ D_1(X) \\ E_1(X) \\ F_1(X) \\ H_1(X) \end{Bmatrix} = \begin{Bmatrix} (1+u_{,X})N + M_y\theta_{Y,X} + M_z\theta_{Z,X} - T_y\theta_Z + T_z\theta_Y \\ Nv_{,X} + T_y \\ Nw_{,X} + T_z \\ T_z(1+u_{,X}) + Q_4\theta_{Y,X} + Q_7\theta_{Z,X} + Q_9\theta_Y + Q_{10}\theta_Z \\ M_y(1+u_{,X}) + Q_1\theta_{Z,X} + Q_2\theta_{Y,X} + Q_3\theta_Z + Q_4\theta_Y \\ -T_y(1+u_{,X}) + Q_3\theta_{Y,X} + Q_6\theta_{Z,X} + Q_8\theta_Z + Q_{10}\theta_Y \\ M_z(1+u_{,X}) + Q_5\theta_{Z,X} + Q_1\theta_{Y,X} + Q_6\theta_Z + Q_7\theta_Y \end{Bmatrix}$$

$$G(X)] = \begin{bmatrix} (\kappa_u N_{u_{,X}})^T & 0 & 0 & 0 & 0 \\ 0 & (\kappa_v N_{v_{,X}})^T & 0 & 0 & 0 \\ 0 & 0 & (\kappa_w N_{w_{,X}})^T & 0 & 0 \\ 0 & 0 & 0 & (\kappa_{\theta_Y} N_{\theta_Y})^T & 0 \\ 0 & 0 & 0 & (\kappa_{\theta_Y} N_{\theta_{Y,X}})^T & 0 \\ 0 & 0 & 0 & 0 & (\kappa_{\theta_Z} N_{\theta_Z})^T \\ 0 & 0 & 0 & 0 & (\kappa_{\theta_Z} N_{\theta_{Z,X}})^T \end{bmatrix}$$

$$[T_1(X)] = \begin{bmatrix} (\kappa_u N_{u_{,X}})^T & 0 & 0 & 0 & 0 \\ 0 & (\kappa_v N_{v_{,X}})^T & 0 & 0 & 0 \\ 0 & 0 & (\kappa_w N_{w_{,X}})^T & 0 & 0 \\ 0 & 0 & 0 & (\kappa_{\theta_Y} N_{\theta_Y})^T & 0 \\ 0 & 0 & 0 & 0 & (\kappa_{\theta_Z} N_{\theta_Z})^T \end{bmatrix}$$

$$[T_2(X)] = \begin{bmatrix} (\kappa_u N_u)^T & 0 & 0 & 0 & 0 \\ 0 & (\kappa_v N_v)^T & 0 & 0 & 0 \\ 0 & 0 & (\kappa_w N_w)^T & 0 & 0 \\ 0 & 0 & 0 & (\kappa_{\theta_Y} N_{\theta_Y})^T & 0 \\ 0 & 0 & 0 & 0 & (\kappa_{\theta_Z} N_{\theta_Z})^T \end{bmatrix}$$

The element nodal concentrated loads vector

$$F^e = \begin{bmatrix} F^e_{X1} & F^e_{Y1} & F^e_{Z1} & M^e_{Y1} & M^e_{Z1} & F^e_{X2} & F^e_{Y2} & F^e_{Z2} & M^e_{Y2} & M^e_{Z2} & F^e_{X3} & F^e_{Y3} & F^e_{Z3} & M^e_{Y3} & M^e_{Z3} \end{bmatrix}^T$$

$$[\Omega_{int}(X)] = \begin{bmatrix} \frac{\partial A_1}{\partial u_X} & \frac{\partial A_1}{\partial v_X} & \frac{\partial A_1}{\partial w_X} & \frac{\partial A_1}{\partial \theta_Y} & \frac{\partial A_1}{\partial \theta_{Y,X}} & \frac{\partial A_1}{\partial \theta_Z} & \frac{\partial A_1}{\partial \theta_{Z,X}} \\ \frac{\partial B_1}{\partial u_X} & \frac{\partial B_1}{\partial v_X} & \frac{\partial B_1}{\partial w_X} & \frac{\partial B_1}{\partial \theta_Y} & \frac{\partial B_1}{\partial \theta_{Y,X}} & \frac{\partial B_1}{\partial \theta_Z} & \frac{\partial B_1}{\partial \theta_{Z,X}} \\ \frac{\partial C_1}{\partial u_X} & \frac{\partial C_1}{\partial v_X} & \frac{\partial C_1}{\partial w_X} & \frac{\partial C_1}{\partial \theta_Y} & \frac{\partial C_1}{\partial \theta_{Y,X}} & \frac{\partial C_1}{\partial \theta_Z} & \frac{\partial C_1}{\partial \theta_{Z,X}} \\ \frac{\partial D_1}{\partial u_X} & \frac{\partial D_1}{\partial v_X} & \frac{\partial D_1}{\partial w_X} & \frac{\partial D_1}{\partial \theta_Y} & \frac{\partial D_1}{\partial \theta_{Y,X}} & \frac{\partial D_1}{\partial \theta_Z} & \frac{\partial D_1}{\partial \theta_{Z,X}} \\ \frac{\partial E_1}{\partial u_X} & \frac{\partial E_1}{\partial v_X} & \frac{\partial E_1}{\partial w_X} & \frac{\partial E_1}{\partial \theta_Y} & \frac{\partial E_1}{\partial \theta_{Y,X}} & \frac{\partial E_1}{\partial \theta_Z} & \frac{\partial E_1}{\partial \theta_{Z,X}} \\ \frac{\partial F_1}{\partial u_X} & \frac{\partial F_1}{\partial v_X} & \frac{\partial F_1}{\partial w_X} & \frac{\partial F_1}{\partial \theta_Y} & \frac{\partial F_1}{\partial \theta_{Y,X}} & \frac{\partial F_1}{\partial \theta_Z} & \frac{\partial F_1}{\partial \theta_{Z,X}} \\ \frac{\partial H_1}{\partial u_X} & \frac{\partial H_1}{\partial v_X} & \frac{\partial H_1}{\partial w_X} & \frac{\partial H_1}{\partial \theta_Y} & \frac{\partial H_1}{\partial \theta_{Y,X}} & \frac{\partial H_1}{\partial \theta_Z} & \frac{\partial H_1}{\partial \theta_{Z,X}} \end{bmatrix}$$

$$[\Omega_{ext}] = \begin{bmatrix} 0 & 0 & 0 & 0 & 0 & 0 & 0 \\ 0 & 0 & 0 & 0 & 0 & F_p & 0 \\ 0 & 0 & 0 & -F_p & 0 & 0 & 0 \\ 0 & 0 & -F_p & 0 & 0 & 0 & 0 \\ 0 & 0 & 0 & 0 & 0 & 0 & 0 \\ 0 & F_p & 0 & 0 & 0 & 0 & 0 \\ 0 & 0 & 0 & 0 & 0 & 0 & 0 \end{bmatrix}$$

The classical shape functions used in Section 3 are:

$$N_1(\xi) = \frac{1}{2}\xi(\xi-1)$$
$$N_2(\xi) = 1-\xi^2$$
$$N_3(\xi) = \frac{1}{2}\xi(\xi+1)$$

where $\xi = 2\frac{X}{l^e_o} - 1$, X is the local coordinate along the beam element axis ($X \in [0, l^e_o]$), l^e_o the element reference length and $\xi \in [-1,1]$, the reference coordinate of the points on the beam element.

$$N_u = [N_1 \;\; 0 \;\; 0 \;\; 0 \;\; 0 \;\; N_2 \;\; 0 \;\; 0 \;\; 0 \;\; 0 \;\; N_3 \;\; 0 \;\; 0 \;\; 0 \;\; 0]^T$$
$$N_v = [0 \;\; N_1 \;\; 0 \;\; 0 \;\; 0 \;\; 0 \;\; N_2 \;\; 0 \;\; 0 \;\; 0 \;\; 0 \;\; N_3 \;\; 0 \;\; 0 \;\; 0]^T$$
$$N_w = [0 \;\; 0 \;\; N_1 \;\; 0 \;\; 0 \;\; 0 \;\; 0 \;\; N_2 \;\; 0 \;\; 0 \;\; 0 \;\; 0 \;\; N_3 \;\; 0 \;\; 0]^T$$
$$N_{\theta_Y} = [0 \;\; 0 \;\; 0 \;\; N_1 \;\; 0 \;\; 0 \;\; 0 \;\; 0 \;\; N_2 \;\; 0 \;\; 0 \;\; 0 \;\; 0 \;\; N_3 \;\; 0]^T$$
$$N_{\theta_Z} = [0 \;\; 0 \;\; 0 \;\; 0 \;\; N_1 \;\; 0 \;\; 0 \;\; 0 \;\; 0 \;\; N_2 \;\; 0 \;\; 0 \;\; 0 \;\; 0 \;\; N_3]^T$$

$$\kappa_u = \begin{bmatrix} 1 & 0 & 0 & 0 & 0 & 0 & 0 & 0 & 0 & 0 & 0 & 0 & 0 & 0 & 0 \\ 0 & 0 & 0 & 0 & 0 & 1 & 0 & 0 & 0 & 0 & 0 & 0 & 0 & 0 & 0 \\ 0 & 0 & 0 & 0 & 0 & 0 & 0 & 0 & 0 & 0 & 1 & 0 & 0 & 0 & 0 \end{bmatrix}$$

$$\kappa_v = \begin{bmatrix} 0 & 1 & 0 & 0 & 0 & 0 & 0 & 0 & 0 & 0 & 0 & 0 & 0 & 0 & 0 \\ 0 & 0 & 0 & 0 & 0 & 0 & 1 & 0 & 0 & 0 & 0 & 0 & 0 & 0 & 0 \\ 0 & 0 & 0 & 0 & 0 & 0 & 0 & 0 & 0 & 0 & 0 & 1 & 0 & 0 & 0 \end{bmatrix}$$

$$\kappa_w = \begin{bmatrix} 0 & 0 & 1 & 0 & 0 & 0 & 0 & 0 & 0 & 0 & 0 & 0 & 0 & 0 & 0 \\ 0 & 0 & 0 & 0 & 0 & 0 & 0 & 1 & 0 & 0 & 0 & 0 & 0 & 0 & 0 \\ 0 & 0 & 0 & 0 & 0 & 0 & 0 & 0 & 0 & 0 & 0 & 0 & 1 & 0 & 0 \end{bmatrix}$$

$$\kappa_{\theta_Y} = \begin{bmatrix} 0 & 0 & 0 & 0 & 1 & 0 & 0 & 0 & 0 & 0 & 0 & 0 & 0 & 0 & 0 \\ 0 & 0 & 0 & 0 & 0 & 0 & 0 & 0 & 1 & 0 & 0 & 0 & 0 & 0 & 0 \\ 0 & 0 & 0 & 0 & 0 & 0 & 0 & 0 & 0 & 0 & 0 & 0 & 0 & 1 & 0 \end{bmatrix}$$

$$\kappa_{\theta_Z} = \begin{bmatrix} 0 & 0 & 0 & 0 & 0 & 1 & 0 & 0 & 0 & 0 & 0 & 0 & 0 & 0 & 0 \\ 0 & 0 & 0 & 0 & 0 & 0 & 0 & 0 & 0 & 1 & 0 & 0 & 0 & 0 & 0 \\ 0 & 0 & 0 & 0 & 0 & 0 & 0 & 0 & 0 & 0 & 0 & 0 & 0 & 0 & 1 \end{bmatrix}$$

$$[G]^T = \begin{bmatrix} \frac{1}{l^e_o}(2\xi-1) & 0 & 0 & 0 & 0 & 0 & 0 \\ 0 & \frac{1}{l^e_o}(2\xi-1) & 0 & 0 & 0 & 0 & 0 \\ 0 & 0 & \frac{1}{l^e_o}(2\xi-1) & 0 & 0 & 0 & 0 \\ 0 & 0 & 0 & \frac{1}{2}\xi(\xi-1) & \frac{1}{l^e_o}(2\xi-1) & 0 & 0 \\ 0 & 0 & 0 & 0 & 0 & \frac{1}{2}\xi(\xi-1) & \frac{1}{l^e_o}(2\xi-1) \\ -\frac{4}{l^e_o}\xi & 0 & 0 & 0 & 0 & 0 & 0 \\ 0 & -\frac{4}{l^e_o}\xi & 0 & 0 & 0 & 0 & 0 \\ 0 & 0 & -\frac{4}{l^e_o}\xi & 0 & 0 & 0 & 0 \\ 0 & 0 & 0 & 1-\xi^2 & -\frac{4}{l^e_o}\xi & 0 & 0 \\ 0 & 0 & 0 & 0 & 0 & 1-\xi^2 & -\frac{4}{l^e_o}\xi \\ \frac{1}{l^e_o}(2\xi+1) & 0 & 0 & 0 & 0 & 0 & 0 \\ 0 & \frac{1}{l^e_o}(2\xi+1) & 0 & 0 & 0 & 0 & 0 \\ 0 & 0 & \frac{1}{l^e_o}(2\xi+1) & 0 & 0 & 0 & 0 \\ 0 & 0 & 0 & \frac{1}{2}\xi(\xi+1) & \frac{1}{l^e_o}(2\xi+1) & 0 & 0 \\ 0 & 0 & 0 & 0 & 0 & \frac{1}{2}\xi(\xi+1) & \frac{1}{l^e_o}(2\xi+1) \end{bmatrix}$$

$$[T_1]^T = \begin{bmatrix} \frac{1}{l_o^e}(2\xi-1) & 0 & 0 & 0 & 0 \\ 0 & \frac{1}{l_o^e}(2\xi-1) & 0 & 0 & 0 \\ 0 & 0 & \frac{1}{l_o^e}(2\xi-1) & 0 & 0 \\ 0 & 0 & 0 & \frac{1}{2}\xi(\xi-1) & 0 \\ 0 & 0 & 0 & 0 & \frac{1}{2}\xi(\xi-1) \\ -\frac{4}{l_o^e}\xi & 0 & 0 & 0 & 0 \\ 0 & -\frac{4}{l_o^e}\xi & 0 & 0 & 0 \\ 0 & 0 & -\frac{4}{l_o^e}\xi & 0 & 0 \\ 0 & 0 & 0 & 1-\xi^2 & 0 \\ 0 & 0 & 0 & 0 & 1-\xi^2 \\ \frac{1}{l_o^e}(2\xi+1) & 0 & 0 & 0 & 0 \\ 0 & \frac{1}{l_o^e}(2\xi+1) & 0 & 0 & 0 \\ 0 & 0 & \frac{1}{l_o^e}(2\xi+1) & 0 & 0 \\ 0 & 0 & 0 & \frac{1}{2}\xi(\xi+1) & 0 \\ 0 & 0 & 0 & 0 & \frac{1}{2}\xi(\xi+1) \end{bmatrix}$$

$$[T_2]^T = \begin{bmatrix} \frac{1}{2}\xi(\xi-1) & 0 & 0 & 0 & 0 \\ 0 & \frac{1}{2}\xi(\xi-1) & 0 & 0 & 0 \\ 0 & 0 & \frac{1}{2}\xi(\xi-1) & 0 & 0 \\ 0 & 0 & 0 & \frac{1}{2}\xi(\xi-1) & 0 \\ 0 & 0 & 0 & 0 & \frac{1}{2}\xi(\xi-1) \\ 1-\xi^2 & 0 & 0 & 0 & 0 \\ 0 & 1-\xi^2 & 0 & 0 & 0 \\ 0 & 0 & 1-\xi^2 & 0 & 0 \\ 0 & 0 & 0 & 1-\xi^2 & 0 \\ 0 & 0 & 0 & 0 & 1-\xi^2 \\ \frac{1}{2}\xi(\xi+1) & 0 & 0 & 0 & 0 \\ 0 & \frac{1}{2}\xi(\xi+1) & 0 & 0 & 0 \\ 0 & 0 & \frac{1}{2}\xi(\xi+1) & 0 & 0 \\ 0 & 0 & 0 & \frac{1}{2}\xi(\xi+1) & 0 \\ 0 & 0 & 0 & 0 & \frac{1}{2}\xi(\xi+1) \end{bmatrix}$$

External dead loads vector

$$F_{ext}^d = \left[\frac{f_x l_o^e}{6} + F_{X1}^e \quad \frac{f_y l_o^e}{6} + F_{Y1}^e \quad \frac{f_z l_o^e}{6} + F_{Z1}^e \quad M_{Y1}^e \quad M_{Z1}^e \quad \frac{2f_x l_o^e}{3} + F_{X2}^e \quad \frac{2f_y l_o^e}{3} + F_{Y2}^e \quad \frac{2f_z l_o^e}{3} + F_{Z2}^e \quad M_{Y2}^e \quad M_{Z2}^e \quad \frac{f_x l_o^e}{6} + F_{X3}^e \quad \frac{f_y l_o^e}{6} + F_{Y3}^e \quad \frac{f_z l_o^e}{6} + F_{Z3}^e \quad M_{Y3}^e \quad M_{Z3}^e \right]^T$$

External loads vector due to the inflation pressure

$$\frac{F_{ext}^p}{F_p} = \begin{bmatrix} -1 & -\frac{1}{6}(3\theta_{Z1}^e + 4\theta_{Z2}^e - \theta_{Z3}^e) & \frac{1}{6}(3\theta_{Y1}^e + 4\theta_{Y2}^e - \theta_{Y3}^e) & \frac{1}{6}(3W_1^e - 4W_2^e + W_3^e) & -\frac{1}{6}(3V_1^e - 4V_2^e + V_3^e) & 0 & \frac{2}{3}(\theta_{Z1}^e - \theta_{Z3}^e) & -\frac{2}{3}(\theta_{Y1}^e - \theta_{Y3}^e) & \frac{2}{3}(W_1^e - W_3^e) & -\frac{2}{3}(V_1^e - V_3^e) & 1 \\ & \frac{1}{6}(-\theta_{Z1}^e + 4\theta_{Z2}^e + 3\theta_{Z3}^e) & -\frac{1}{6}(-\theta_{Y1}^e + 4\theta_{Y2}^e + 3\theta_{Y3}^e) & -\frac{1}{6}(W_1^e - 4W_2^e + 3W_3^e) & \frac{1}{6}(V_1^e - 4V_2^e + 3V_3^e) & & & & & & \end{bmatrix}^T$$

Appendix B. Elements of stiffness matrix

The elements in the 'upper-triangle' part of the symmetric linear stiffness matrix of an inflatable three-noded Timoshenko beam with full integration are given bellow; entries not shown are zeros:

$$K_{1,1} = \frac{7}{3l_o}(N^o + C_{11}A_o)$$
$$K_{1,6} = \frac{-8}{3l_o}(N^o + C_{11}A_o)$$
$$K_{1,11} = \frac{1}{3l_o}(N^o + C_{11}A_o)$$
$$K_{2,2} = \frac{7}{3l_o}\left(N^o + \frac{1}{2}k_y A_o C_{66}\right)$$
$$K_{2,5} = \frac{1}{2}\left(F_p + \frac{1}{2}k_y A_o C_{66}\right)$$
$$K_{2,7} = -\frac{8}{3l_o}\left(N^o + \frac{1}{2}k_y A_o C_{66}\right)$$
$$K_{2,10} = \frac{2}{3}\left(F_p + \frac{1}{2}k_y A_o C_{66}\right)$$
$$K_{2,12} = \frac{1}{3l_o}\left(N^o + \frac{1}{2}k_y A_o C_{66}\right)$$
$$K_{2,15} = -\frac{1}{6}\left(F_p + \frac{1}{2}k_y A_o C_{66}\right)$$
$$K_{3,3} = \frac{7}{3l_o}\left(N^o + \frac{1}{2}k_z A_o C_{66}\right)$$
$$K_{3,4} = -\frac{1}{2}\left(F_p + \frac{1}{2}k_z A_o C_{66}\right)$$
$$K_{3,8} = -\frac{8}{3l_o}\left(N^o + \frac{1}{2}k_z A_o C_{66}\right)$$
$$K_{3,9} = -\frac{2}{3}\left(F_p + \frac{1}{2}k_z A_o C_{66}\right)$$
$$K_{3,13} = \frac{1}{3l_o}\left(N^o + \frac{1}{2}k_z A_o C_{66}\right)$$
$$K_{3,14} = \frac{1}{6}\left(F_p + \frac{1}{2}k_z A_o C_{66}\right)$$
$$K_{4,4} = \frac{7}{3l_o}\left(C_{11} + \frac{N^o}{A_o}\right)I_o + \frac{2l_o}{15}\left(N^o + \frac{1}{2}k_z A_o C_{66}\right)$$
$$K_{4,8} = \frac{2}{3}\left(F_p + \frac{1}{2}k_z A_o C_{66}\right)$$
$$K_{4,9} = -\frac{8}{3l_o}\left(C_{11} + \frac{N^o}{A_o}\right)I_o + \frac{l_o}{15}\left(N^o + \frac{1}{2}k_z A_o C_{66}\right)$$
$$K_{4,13} = -\frac{1}{6}\left(F_p + \frac{1}{2}k_z A_o C_{66}\right)$$
$$K_{4,14} = \frac{1}{3l_o}\left(C_{11} + \frac{N^o}{A_o}\right)I_o - \frac{l_o}{30}\left(N^o + \frac{1}{2}k_z A_o C_{66}\right)$$

$$K_{5,5} = \frac{7}{3l_o}\left(C_{11} + \frac{N^o}{A_o}\right)I_o + \frac{2l_o}{15}\left(N^o + \frac{1}{2}k_yA_oC_{66}\right)$$

$$K_{5,7} = -\frac{2}{3}\left(F_p + \frac{1}{2}k_yA_oC_{66}\right)$$

$$K_{5,10} = -\frac{8}{3l_o}\left(C_{11} + \frac{N^o}{A_o}\right)I_o + \frac{l_o}{15}\left(N^o + \frac{1}{2}k_yA_oC_{66}\right)$$

$$K_{5,12} = \frac{1}{6}\left(F_p + \frac{1}{2}k_yA_oC_{66}\right)$$

$$K_{5,15} = \frac{1}{3l_o}\left(C_{11} + \frac{N^o}{A_o}\right)I_o - \frac{l_o}{30}\left(N^o + \frac{1}{2}k_yA_oC_{66}\right)$$

$$K_{6,6} = \frac{16}{3l_o}(N^o + C_{11}A_o)$$

$$K_{6,11} = -\frac{8}{3l_o}(N^o + C_{11}A_o)$$

$$K_{7,7} = \frac{16}{3l_o}\left(N^o + \frac{1}{2}k_yA_oC_{66}\right)$$

$$K_{7,12} = -\frac{8}{3l_o}\left(N^o + \frac{1}{2}k_yA_oC_{66}\right)$$

$$K_{7,15} = \frac{2}{3}\left(F_p + \frac{1}{2}k_yA_oC_{66}\right)$$

$$K_{8,8} = \frac{16}{3l_o}\left(N^o + \frac{1}{2}k_zA_oC_{66}\right)$$

$$K_{8,13} = -\frac{8}{3l_o}\left(N^o + \frac{1}{2}k_zA_oC_{66}\right)$$

$$K_{8,14} = -\frac{2}{3}\left(F_p + \frac{1}{2}k_zA_oC_{66}\right)$$

$$K_{9,9} = \frac{16}{3l_o}\left(C_{11} + \frac{N^o}{A_o}\right)I_o + \frac{8l_o}{15}\left(N^o + \frac{1}{2}k_zA_oC_{66}\right)$$

$$K_{9,13} = \frac{2}{3}\left(F_p + \frac{1}{2}k_zA_oC_{66}\right)$$

$$K_{9,14} = -\frac{8}{3l_o}\left(C_{11} + \frac{N^o}{A_o}\right)I_o + \frac{l_o}{15}\left(N^o + \frac{1}{2}k_zA_oC_{66}\right)$$

$$K_{10,10} = \frac{16}{3l_o}\left(C_{11} + \frac{N^o}{A_o}\right)I_o + \frac{8l_o}{15}\left(N^o + \frac{1}{2}k_yA_oC_{66}\right)$$

$$K_{10,12} = -\frac{2}{3}\left(F_p + \frac{1}{2}k_yA_oC_{66}\right)$$

$$K_{10,15} = -\frac{8}{3l_o}\left(C_{11} + \frac{N^o}{A_o}\right)I_o + \frac{l_o}{15}\left(N^o + \frac{1}{2}k_yA_oC_{66}\right)$$

$$K_{11,11} = \frac{7}{3l_o}(N^o + C_{11}A_o)$$

$$K_{12,12} = \frac{7}{3l_o}\left(N^o + \frac{1}{2}k_yA_oC_{66}\right)$$

$$K_{12,15} = -\frac{1}{2}\left(F_p + \frac{1}{2}k_yA_oC_{66}\right)$$

$$K_{13,13} = \frac{7}{3l_o}\left(N^o + \frac{1}{2}k_zA_oC_{66}\right)$$

$$K_{13,14} = \frac{1}{2}\left(F_p + \frac{1}{2}k_zA_oC_{66}\right)$$

$$K_{14,14} = \frac{7}{3l_o}\left(C_{11} + \frac{N^o}{A_o}\right)I_o + \frac{2l_o}{15}\left(N^o + \frac{1}{2}k_zA_oC_{66}\right)$$

$$K_{15,15} = \frac{7}{3l_o}\left(C_{11} + \frac{N^o}{A_o}\right)I_o + \frac{2l_o}{15}\left(N^o + \frac{1}{2}k_yA_oC_{66}\right)$$

The elements of the symmetric linear stiffness matrix of an inflatable three-noded Timoshenko beam with reduced integration are given bellow; elements not shown are equal to the elements in the full integration case:

$$K_{4,4} = \frac{7}{3l_o}\left(C_{11} + \frac{N^o}{A_o}\right)I_o + \frac{l_o}{9}\left(N^o + \frac{1}{2}k_zA_oC_{66}\right)$$

$$K_{4,9} = -\frac{8}{3l_o}\left(C_{11} + \frac{N^o}{A_o}\right)I_o + \frac{l_o}{9}\left(N^o + \frac{1}{2}k_zA_oC_{66}\right)$$

$$K_{4,14} = \frac{1}{3l_o}\left(C_{11} + \frac{N^o}{A_o}\right)I_o - \frac{l_o}{18}\left(N^o + \frac{1}{2}k_zA_oC_{66}\right)$$

$$K_{5,5} = \frac{7}{3l_o}\left(C_{11} + \frac{N^o}{A_o}\right)I_o + \frac{l_o}{9}\left(N^o + \frac{1}{2}k_yA_oC_{66}\right)$$

$$K_{5,10} = -\frac{8}{3l_o}\left(C_{11} + \frac{N^o}{A_o}\right)I_o + \frac{l_o}{9}\left(N^o + \frac{1}{2}k_yA_oC_{66}\right)$$

$$K_{5,15} = \frac{1}{3l_o}\left(C_{11} + \frac{N^o}{A_o}\right)I_o - \frac{l_o}{18}\left(N^o + \frac{1}{2}k_yA_oC_{66}\right)$$

$$K_{9,9} = \frac{16}{3l_o}\left(C_{11} + \frac{N^o}{A_o}\right)I_o + \frac{4l_o}{9}\left(N^o + \frac{1}{2}k_zA_oC_{66}\right)$$

$$K_{9,14} = -\frac{8}{3l_o}\left(C_{11} + \frac{N^o}{A_o}\right)I_o + \frac{l_o}{9}\left(N^o + \frac{1}{2}k_zA_oC_{66}\right)$$

$$K_{10,10} = \frac{16}{3l_o}\left(C_{11} + \frac{N^o}{A_o}\right)I_o + \frac{4l_o}{9}\left(N^o + \frac{1}{2}k_yA_oC_{66}\right)$$

$$K_{10,15} = -\frac{8}{3l_o}\left(C_{11} + \frac{N^o}{A_o}\right)I_o + \frac{l_o}{9}\left(N^o + \frac{1}{2}k_yA_oC_{66}\right)$$

$$K_{14,14} = \frac{7}{3l_o}\left(C_{11} + \frac{N^o}{A_o}\right)I_o + \frac{l_o}{9}\left(N^o + \frac{1}{2}k_zA_oC_{66}\right)$$

$$K_{15,15} = \frac{7}{3l_o}\left(C_{11} + \frac{N^o}{A_o}\right)I_o + \frac{l_o}{9}\left(N^o + \frac{1}{2}k_yA_oC_{66}\right)$$

References

Apedo, K.L., Ronel, S., Jacquelin, E., Massenzio, M., Bennani, A., 2009. Theoretical analysis of inflatable beams made from orthotropic fabric. Thin-Walled Structures 47, 1507–1522.

Aravas, N., 1992. Finite elastoplastic transformations of transversely isotropic metals. International Journal of Solids and Structures 29, 2137–2157.

Batoz, J.M., Dhatt, G., 1990. Modélisation des Structures par Eléments Finis.

Berry, D.T., Yang, H.T.Y., 1996. Formulation and experimental verification of a pneumatic finite element. International Journal for Numerical Methods in Engineering 39 (1), 1097–1114.

Bhatti, M.A., 2006. Advanced Topics in Finite Element Analysis of Structures with Mathematica and MATLAB Computations. John Wiley & Sons, New York (NY).

Bouzidi, R., Ravaut, Y., Wielgosz, C., 2003. Finite elements for 2d problems of pressurized membranes. Computers and Structures 81, 2479–2490.

Cavallaro, P., Sadegh, A., 2006. Air-inflated fabric structures, 11th ed.. In: Avallone, E., , Baumeister, T., III, Sadegh, A. (Eds.), Marks Standard Handbook for Mechanical Engineers McGraw-Hill Publication, pp. 20–116. Chapter 20.10.

Cavallaro, P.V., Johnson, M.E., Sadegh, A.M., 2003. Mechanics of plain-woven fabrics for inflated structures. Composite Structures 61, 375–393.

Cavallaro, P.V., Sadegh, A.M., Quigley, C.J., 2007. Contributions of strain energy and PV-work on the bending behavior of uncoated plain-woven fabric air beams. Journal of Engineered Fibers and Fabrics 2 (1), 16–30.

Cheng, X., Xiong, J.J., 2009. A novel analytical model for predicting the compression modulus of 2d PWF composites. Composite Structures 88, 296–303.

Comer, R.L., Levy, S., 1963. Deflections of an inflated circular-cylindrical cantilever beam. AIAA Journal 1 (7), 1652–1655.

Davids, W.G., 2007. Finite-element analysis of tubular fabric beams including pressure effects and local fabric wrinkling. Finite Elements in Analysis and Design 44, 24–33.

Davids, W.G., Zhang, H., 2008. Beam finite element for nonlinear analysis of pressurized fabric beam-columns. Engineering Structures 30, 1969–1980.

Fichter, W.B., 1966. A theory for inflated thin wall cylindrical beams. Technical Report, NASA Technical Note, NASA TND- 3466.

Friedman, Z., Kosmatka, J.B., 1993. An improved two-noded Timoshenko beam finite element. Computers and Structures 47 (3), 473–481.

Harursampath, D., Hodges, D.H., 1999. Asymptotic analysis of the non-linear behavior of long anisotropic tubes. International Journal of Non-Linear Mechanics 34, 1003–1018.

Houliara, S., Karamanos, S.A., 2006. Buckling and post-buckling of long pressurized elastic thin-walled tubes under in-plane bending. International Journal of Non-Linear Mechanics 41, 491–511.

Houliara, S., Karamanos, S.A., 2010. Stability of long transversely-isotropic elastic cylindrical shells under bending. International Journal of Solids and Structures 47, 10–24.

Le Van, A., Wielgosz, C., 2005. Bending and buckling of inflatable beams: some new theoretical results. Thin-Walled Structures 43, 1166–1187.

Le Van, A., Wielgosz, C., 2007. Finite element formulation for inflatable beams. Thin-Walled Structures 45, 221–236.
Main, J.A., Peterson, S.W., Strauss, A.M., 1995. Beam-type bending of space-based membrane structures. Journal of Aerospace Engineering 8 (2), 120–125.
Malm, C.G., Davids, W.G., Peterson, M.L., Turner, A.W., 2009. Experimental characterization and finite element analysis of inflated fabric beams. Construction and Building Materials 23, 2027–2034.
Molloy, S.J., 1998. Finite element analysis of a pair of leaning pressurized arch-shells under snow and wind loads. Master's thesis, Virginia Polytechnic Institute and State University, Blacksburg, VA.
Molloy, S.J., Plaut, R.H., Kim, J.Y., 1999. Behavior of pair of leaning arch-shells under snow and wind loads. Journal of Engineering Mechanics 125, 663–667.
Plaut, R.H., Goh, J.K.S., Kigudde, M., Hammerand, D.C., 2000. Shell analysis of an inflatable arch subjected to snow and wind loading. International Journal of Solids and Structures 37, 4275–4288.
Quigley, C., Cavallaro, P.V., Johnson, A.R., Sadegh, A.M., 2003. Advances in fabric and structural analyses of pressure inflated structures. In: Proceedings of the ASME Textile Division. American Society of Mechanical Engineers, New York.
Spencer, A.J.M., 1972. Deformations of Fiber-Reinforced Materials. Oxford University Press, Oxford.
Spencer, A.J.M., 1984. Constitutive theory for strongly anisotropic materials in continuum theory of the mechanics of fiber-reinforced composites. In: Spencer, A.J.M. (Ed.), Courses and Lectures, International Center for Mechanical Sciences, vol. 282. Springer, Berlin,Udine, pp. 1–32.
Steeves, E.C., 1975. A linear analysis of the deformation of pressure stabilized beams. Technical Report, US Army, Technical Report AND-006-493.
Steeves, E.C., 1978. Structural behavior of pressure stabilized arches. Technical Report, Technical Report Natick/TR-78/018, U.S. Army Natick Research and Development, Laboratory, Natick, MA.
Suhey, J.D., Kim, N.H., Niezrecki, C., 2005. Numerical modeling and design of inflatable structures – application to open-ocean-aquaculture cages. Aquacultural Engineering 33, 285–303.
Thomas, J.C., Wielgosz, C., 2004. Deflections of highly inflated fabric tubes. Thin-Walled Structures 42, 1049–1066.
Veldman, S.L., Bergsma, O.K., Beukers, A., 2005. Bending of anisotropic inflated cylindrical beams. Thin-Walled Structures 43, 461–475.
Vysochina, K., 2005. Comportement des textiles techniques souples dans le domaine des grandes déformations: indentification de la rigidité en cisaillement plan. Ph.D. thesis, Université Claude Bernard Lyon 1.
Webber, J.P.H., 1982. Deflections of inflated cylindrical cantilever beams subjected to bending and torsion. Aeronautical Journal 86 (858), 306–312.
Wielgosz, C., Thomas, J.C., 2002. Deflection of inflatable fabric panels at high pressure. Thin-Walled Structures 40, 523–536.
Wielgosz, C., Thomas, J.C., 2003. An inflatable fabric beam finite element. Communications in Numerical Methods in Engineering 19, 307–312.